

Causal Deep Reinforcement Learning Using Observational Data

Wenxuan Zhu¹, Chao Yu^{2*} and Qiang Zhang^{1*}

¹Dalian University of Technology

²Sun Yat-sen University

zhuwenxuan@mail.dlut.edu.cn, yuchao3@mail.sysu.edu.cn, zhangq@dlut.edu.cn

Abstract

Deep reinforcement learning (DRL) requires the collection of interventional data, which is sometimes expensive and even unethical in the real world, such as in the autonomous driving and the medical field. Offline reinforcement learning promises to alleviate this issue by exploiting the vast amount of observational data available in the real world. However, observational data may mislead the learning agent to undesirable outcomes if the behavior policy that generates the data depends on unobserved random variables (i.e., confounders). In this paper, we propose two deconfounding methods in DRL to address this problem. The methods first calculate the importance degree of different samples based on the causal inference technique, and then adjust the impact of different samples on the loss function by reweighting or resampling the offline dataset to ensure its unbiasedness. These deconfounding methods can be flexibly combined with existing model-free DRL algorithms such as soft actor-critic and deep Q-learning, provided that a weak condition can be satisfied by the loss functions of these algorithms. We prove the effectiveness of our deconfounding methods and validate them experimentally.

1 Introduction

Human beings can learn from observation (e.g., in astronomy) and experimentation (e.g., in physics). For example, people understand the laws of astronomy by observing the movements of celestial bodies and the laws of physics by doing physical experiments. Analogously, agents can learn in these two ways as well. In some cases, however, experimentation (i.e., the collection of interventional data) can be expensive and even unethical, while observational data are easy to obtain. For example, it is unsafe for an agent to learn to drive a car on a real road, but we can easily collect data from a human driving a car with sensors.

Reinforcement learning (RL) [Sutton and Barto, 2018] is generally regarded as an interactive learning process, which

means that the agent learns from the interventional data generated by experimentation. As a type of RL methods, offline RL [Kumar *et al.*, 2020; Levine *et al.*, 2020; Siegel *et al.*, 2020; Ernst *et al.*, 2005; Fujimoto *et al.*, 2019; Kumar *et al.*, 2019; Agarwal *et al.*, 2020; Jaques *et al.*, 2019] has been proposed to study how to enable RL algorithms to learn strategies from observational data without interacting with the environment.

Most existing offline RL methods are based on an assumption that $\mathcal{O}_1 = \mathcal{O}_2 = \mathcal{O}_3$, where $o_1 \in \mathcal{O}_1$ denotes the observation of the environment in which the offline data is collected, $o_2 \in \mathcal{O}_2$ denotes the observation in the offline data, and $o_3 \in \mathcal{O}_3$ denotes the observation in the online data where the agent trained using the offline data is tested (In the driving car example, o_1 represents the environmental information perceived by the driver, o_2 represents the environmental information collected by the sensors, and o_3 represents the environmental information perceived by the agent in the testing environment.). This assumption, however, is often difficult to hold in real-world problems. The driver may be able to see more broadly than the sensors, to judge if the road is slippery based on weather conditions, or even to receive traffic conditions around them based on the radio, therefore, it is generally that $\mathcal{O}_1 \neq \mathcal{O}_2$. If the driver makes a decision based on the information not collected by the sensors, i.e., there are unobserved random variables (confounders) that affect the action and the next sensory observation at the same time, the observational data generated by the driver may be misleading. An agent then learns the wrong dynamics of the environment based on this misleading information, leading to a biased estimation of the value functions and the final policies.

Some researches [Sen *et al.*, 2017; Kallus and Zhou, 2018; Wang *et al.*, 2021; Gasse *et al.*, 2021] in recent years study how to train an agent using offline data with the confounders based on the causal inference techniques. However, most of these researches [Sen *et al.*, 2017; Kallus and Zhou, 2018] only target at the bandit problems. Other approaches propose deconfounding methods in RL settings but they are based on certain assumptions such as linear reward/transition functions [Wang *et al.*, 2021], small state spaces [Gasse *et al.*, 2021], or a complex correlation between the features [Wang *et al.*, 2021]. Therefore, these approaches only work for specific types of offline RL algorithms, and cannot be applied to large and continuous environments (See Section 5 for more

*Corresponding author

details.). To address these problems, we propose two kinds of deconfounding methods based on the importance sampling and causal inference techniques. Our deconfounding methods first estimate a conditional distribution density ratio through the least-squares conditional density estimation (LSCDE) [Sugiyama *et al.*, 2010; Rothfuss *et al.*, 2019], and then adjust the impact of different samples on the loss function to ensure the unbiasedness of the loss function. Specifically, we make the following contributions.

- 1) Unlike the existing importance sampling techniques in off-policy evaluation (OPE) [Kallus and Zhou, 2020; Gelada and Bellemare, 2019; Hallak and Mannor, 2017], we estimate a conditional distribution density ratio, which keeps constant in the learning process, and thus can be applied to the RL field.
- 2) In the proposed deconfounding methods, we decouple the deconfounding process from the RL algorithm, i.e., we can uniformly incorporate the conditional distribution density ratio into the loss functions of the offline RL algorithms. In other words, our plug-in deconfounding methods can be combined with existing offline RL algorithms provided that a weak condition is satisfied.
- 3) Furthermore, since we do not learn a latent-based transition model, and do not assume a complex correlation between the features, our deconfounding methods do not contain a complex computational process, and thus can be applied to large and continuous environments.
- 4) We prove theoretically that these two deconfounding methods can construct an unbiased loss function w.r.t. the online data, and thus improve the performance of the offline RL algorithms. The experimental results verify that the proposed deconfounding methods are effective: offline RL algorithms using deconfounding methods perform better on datasets with the confounders.

2 Background

In this section, we define a confounded Markov decision process (CMDP) (similar to [Wang *et al.*, 2021]) and two corresponding structural causal models (SCMs) to describe the RL tasks, in which the offline data include unobserved confounders between the action, reward and next state, and the online data include no confounder between these variables. In specific, there are both continuous random variables \mathbf{X} and discrete random variables \mathbf{Y} in our problems. Without loss of generality, we assume that any discrete random variable belongs to the set of integers. The probability density function $P(\mathbf{x}, \mathbf{y})$ of the discrete and continuous random variables is given as follows:

$$P(\mathbf{x}, \mathbf{y}) = \frac{\partial^p}{\partial x_1 \cdots \partial x_p} \Pr(\mathbf{X} \leq \mathbf{x}, \mathbf{Y} = \mathbf{y}), \quad (1)$$

where $\mathbf{X} \in \mathbb{R}^p$ and $\mathbf{Y} \in \mathbb{Z}^q$. The CMDP for unobserved confounders can be denoted by a nine-tuple $\langle \mathcal{S}, \mathcal{M}, \mathcal{A}, \mathcal{W}, \mathcal{R}, P_1, P_2, P_3, \mu_0 \rangle$, where \mathcal{S} denotes the state space, \mathcal{M} denotes the intermediate state space, \mathcal{A} denotes the discrete action space, \mathcal{W} denotes the confounder space, \mathcal{R} denotes the reward space, $P_1(s', r|s, w, m)$ denotes the dynamics of the CMDP, $P_2(w|s)$ denotes the confounder transition

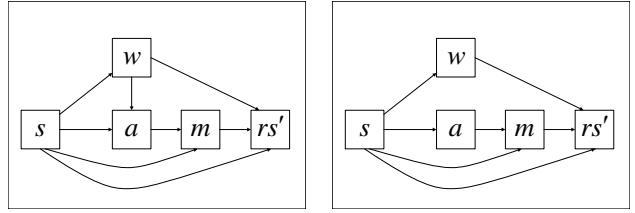


Figure 1: The left and right subfigures represent the SCM in the offline setting and online setting, respectively, which correspond to the CMDP for unobserved confounders. The behavior policy depends on w in the offline setting, but not in the online setting.

distribution, $P_3(m|s, a)$ denotes the intermediate state transition distribution, and $\mu_0(s)$ denotes the initial state distribution. Note that the environment generates the intermediate state m in the process of generating the next state s' . For example, a physician prescribes some drugs to a patient. The actual amount of drugs taken by the patient (i.e., m) may be different from that prescribed by the physician (i.e., a) due to compliance issues. Also note that we integrate the state transition distribution and the reward transition distribution into the dynamics of the CMDP for notational convenience.

The SCM in the offline setting as shown in the first column of Figure 1 can be defined as a four-tuple (U, V, F, P_e) , where U is the exogenous variables, which are not visible in the experiment, V is the endogenous variables, including (s, m, a, w, s', r) , F is the set of structural functions, including the state-reward transition distribution $P_1(s', r|s, w, m)$, the confounder transition distribution $P_2(w|s)$, the intermediate state transition distribution $P_3(m|s, a)$, and the behavior policy $\pi_b(a|s, w)$, and P_e is the distribution of exogenous variables. The positivity assumption here is that, for $m \in \mathcal{M}, a \in \mathcal{A}, s \in \mathcal{S}, w \in \mathcal{W}$ such that $P(s, w) > 0$, $P(m, a|s, w) > 0$. The SCM in the online setting where the agent can intervene on the variable a as shown in the second column of Figure 1 can be defined as another four-tuple (U, V, F, P_e) , where the set of structural functions F includes the state-reward transition distribution $P_1(s', r|s, w, m)$, the confounder transition distribution $P_2(w|s)$, the intermediate state transition distribution $P_3(m|s, a)$, and the policy $\pi(a|s)$. Note, that the policy $\pi(a|s)$ does not depend on w since we assume that w is unobserved to the agent.

3 Confounded Reinforcement Learning

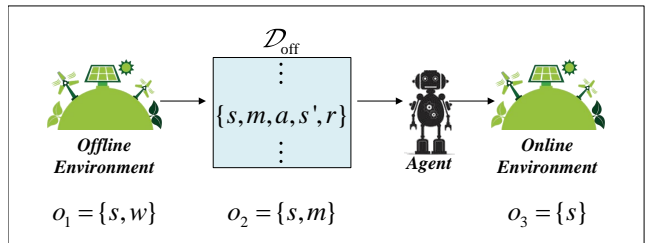


Figure 2: Diagram of the data flow framework, where the confounders in the offline data (i.e., \mathcal{D}_{off}) are unobserved.

Figure 2 describes RL tasks where offline RL algorithms need to use confounded offline data to train an agent that will be tested in the online environment. Specifically, we assume that the observation o_1 of a person/agent in the offline environment includes the state set s and the confounder set w . This person interacts with the environment several times with some fixed strategy. Note that the data generation process in the offline environment conforms to the SCM in the offline setting. At the same time, there are other sensors that keep observing the process of interaction of this person/agent with the environment and gather it into an offline dataset. We assume that the observation o_2 of these sensors includes the state set s and the intermediate state set m . The offline RL algorithms need to utilize the offline dataset to train an agent that will be tested in the online environment, where the observation o_3 includes only the state set s . Note that the online data generation process in the testing environment conforms to the SCM in the online setting. In summary, the confounders are unobserved in both the offline and the online data.

The above task setting leads to different dynamics $\hat{P}(s', r|s, a)$ and $\bar{P}(s', r|s, a)$ in offline data and online data (as proven in Appendix A), where \hat{P} and \bar{P} denote the probability distributions corresponding to the SCMs in the offline and online settings respectively. Because the dynamics in the data determine the optimal value functions, the optimal value functions corresponding to offline data and online data are different. Therefore, if an agent is trained directly by the original deep RL algorithms using the offline data, the estimated optimal value function of this agent is optimal w.r.t. the offline data and suboptimal w.r.t. the online data. Thus, this agent will perform poorly in the online environment. We can also understand the above problem from another perspective, i.e., by analyzing the loss function of the original deep RL algorithms that satisfy Assumption 1.

Assumption 1. The loss function of the neural network (NN) of the deep RL algorithm only depends on the current state s , the action a , the next state s' , and the reward r .

The loss function of the original deep RL algorithms which satisfy Assumption 1 is shown as follows:

$$\begin{aligned} L_1(\phi, \mathcal{D}_{\text{off}}) &\triangleq \mathbb{E}_{s, a, s', r \sim \mathcal{D}_{\text{off}}} [f_\phi + h_\phi] \\ &= \mathbb{E}_{s, a \sim \mathcal{D}_{\text{off}}} \left[\mathbb{E}_{s', r \sim \hat{P}(\cdot, \cdot | s, a)} [f_\phi + h_\phi] \right], \end{aligned} \quad (2)$$

where \mathcal{D}_{off} denotes all offline data collected through observation, ϕ denotes the NN parameters to be optimized, $f_\phi + h_\phi$ denotes the ‘‘loss’’ for a single training sample which differs between different NNs, f_ϕ denotes the part of the ‘‘loss’’ that depends on (s, a, s', r) , and h_ϕ denotes the part of the ‘‘loss’’ that depends only on (s, a) . Table 1 gives some examples of f_ϕ and h_ϕ for different NNs of the deep RL algorithms. It is obvious that the loss function in Equation 2 corresponds to the dynamics in the offline data, and thus the agent trained using this loss function performs poorly in the online environment.

To address this problem, based on importance sampling and do-calculus [Pearl, 2009; Pearl, 2012], we propose two deconfounding methods, namely, reweighting method and resampling method, which can both be combined with existing deep RL algorithms such as soft actor-critic (SAC) [Haarnoja

NN	f_ϕ	h_ϕ
SAC ACTOR	-	$-V(s)$
DQN Q	$(y_1(s', r) - Q_\phi(s, a))^2$	-
DDQN Q	$(y_2(s', r) - Q_\phi(s, a))^2$	-
SAC CRITIC	$(y_3(s', r) - Q_\phi(s, a))^2$	-

Table 1: This table describes the different meanings of f_ϕ and h_ϕ for different NNs. DQN Q, DDQN Q and SAC Critic denote the Q-networks of DQN, DDQN and SAC, respectively. SAC Actor denotes the actor network of SAC. $y_1(s', r) = r + \gamma \max_{a'} Q_{\phi'}(s', a')$. $y_2(s', r) = r + \gamma Q_{\phi'}(s', \arg\max_{a'} Q_{\phi'}(s', a'))$. $y_3(s', r) = r + \gamma (V(s'))$. $V(s) = \pi_\phi(s)^T [Q_\phi(s) - \alpha \log(\pi_\phi(s))]$.

et al., 2017], deep Q-learning (DQN) [Mnih et al., 2013], double deep Q-learning (DDQN) [van Hasselt et al., 2016] and conservative Q-learning (CQL) [Kumar et al., 2020], provided that a weak condition (i.e., Assumption 1) is satisfied. The deconfounding RL algorithms, i.e., the deep RL algorithms combined with the deconfounding methods, can estimate the optimal value function corresponding to the online data, and accordingly the agent trained by these deconfounding RL algorithms is expected to perform well in the online environment. In this section, we assume that the confounders are unobserved in the offline data. We also provide analysis of partially observed confounders in the offline data, and derive the reweighting and resampling methods in Appendix B accordingly.

3.1 Reweighting Method

As mentioned above, since the loss function $L_1(\phi, \mathcal{D}_{\text{off}})$ of the original deep RL algorithms corresponds to the dynamics in the offline data, the agent trained by the original deep RL algorithms performs poorly in the online environment. This inspires us to modify $L_1(\phi, \mathcal{D}_{\text{off}})$ to $L_2(\phi, \mathcal{D}_{\text{off}})$ as follows:

$$L_2(\phi, \mathcal{D}_{\text{off}}) \triangleq \mathbb{E}_{s, a \sim \mathcal{D}_{\text{off}}} \left[\mathbb{E}_{s', r \sim \bar{P}(\cdot, \cdot | s, a)} [f_\phi + h_\phi] \right]. \quad (3)$$

Clearly, $L_2(\phi, \mathcal{D}_{\text{off}})$ corresponds to the dynamics in the online data. However we cannot directly estimate $L_2(\phi, \mathcal{D}_{\text{off}})$ in the form of Equation 3 from the offline data. Therefore, we transform $L_2(\phi, \mathcal{D}_{\text{off}})$ into a form that can be estimated from the offline data as follows:

Proposition 1. Under the definitions of the CMDP and SCMs in Section 2, it holds that

$$\begin{aligned} L_2(\phi, \mathcal{D}_{\text{off}}) &\triangleq \mathbb{E}_{s, a \sim \mathcal{D}_{\text{off}}} \left[\mathbb{E}_{s', r \sim \bar{P}(\cdot, \cdot | s, a)} [f_\phi + h_\phi] \right] \\ &= \mathbb{E}_{s, a \sim \mathcal{D}_{\text{off}}} \left[\mathbb{E}_{s', r, m \sim \hat{P}(\cdot, \cdot, \cdot | s, a)} [d_1(\tau) f_\phi + h_\phi] \right] \\ &= \mathbb{E}_{s, a, s', r, m \sim \mathcal{D}_{\text{off}}} [d_1(\tau) f_\phi + h_\phi], \end{aligned} \quad (4)$$

where τ is a shorthand for the set of variables (s, m, a, s', r) and $d_1(\tau)$ is defined as follows:

$$d_1(\tau) = \frac{\sum_{a'} \hat{P}(s', r | m, a', s) \hat{P}(a' | s)}{\hat{P}(s', r | m, a, s)}. \quad (5)$$

Proof. See Appendix A. \square

As shown in Equation 2 and Equation 4, the only difference between $L_2(\phi, \mathcal{D}_{\text{off}})$ in its new form and $L_1(\phi, \mathcal{D}_{\text{off}})$ is that f_ϕ is multiplied by an extra weight $d_1(\tau)$. Therefore, we only need to estimate $d_1(\tau)$ and modify the loss function of the deep RL algorithms from $L_1(\phi, \mathcal{D}_{\text{off}})$ to $L_2(\phi, \mathcal{D}_{\text{off}})$. Note that $d_1(\tau)$ is composed of several conditional density functions. So, as long as these conditional density functions are estimated from the offline data, we can get an estimate of $d_1(\tau)$. To estimate these conditional density functions containing both discrete and continuous random variables, we adopt the LSCDE technique combined with a trick called *adding jitter* or *jittering* [Nagler, 2018] to add noises to all discrete random variables. It has been theoretically justified that this trick works well if all the noises are chosen from a specific class of noise distribution [Nagler, 2018]. The settings of choosing noises are given in Appendix C.

3.2 Resampling Method

The essence of the reweighting method is to adjust the impact of different samples on the loss function by reweighting the offline data. In other words, by incorporating weights into the loss function, we expand the impact of the samples that are less likely to occur in the offline data than in the online data, i.e., $\hat{P}(s', r|s, a) < \bar{P}(s', r|s, a)$, and vice versa. However, we can also adjust the impact of different samples on the loss function through adjusting the probability that each sample occurs in the offline data. This idea inspires us to define a loss function as follows:

$$L_3(\phi, \mathcal{D}_{\text{off}}) \triangleq \mathbb{E}_{I \sim p_1} [f_{\phi, I} + h_{\phi, I}], \quad (6)$$

where $p_1(I = i) = d_{1,i} / \sum_{j=1}^N d_{1,j}$, $d_{1,i}$ is a shorthand for $d_1(s_i, m_i, a_i, s'_i, r_i)$ where s_i, a_i, r_i, s'_i, m_i denotes the state, action, reward, next state and intermediate state in the offline dataset \mathcal{D}_{off} , respectively, $f_{\phi, I}$ is a shorthand for $f_\phi(s_I, a_I, s'_I, r_I)$ and $h_{\phi, I}$ for $h_\phi(s_I, a_I)$. In $L_3(\phi, \mathcal{D}_{\text{off}})$, we modify the probability that each sample occurs in the offline data according to the value of $d_1(\tau)$. By the definition of $L_3(\phi, \mathcal{D}_{\text{off}})$, based on the importance sampling technique and reparameterization trick, we can prove that the deep RL algorithms combined with the resampling method can also learn the optimal policy w.r.t. the online data from the offline data as follows:

Proposition 2. *Under the definitions of the CMDP and SCMs in Section 2, the loss function of the resampling method is asymptotically equal to that of the reweighting method as in Equation 7 provided that the dataset is large enough.*

$$\lim_{N \rightarrow \infty} (L_3(\phi, \mathcal{D}_{\text{off}}) - L_2(\phi, \mathcal{D}_{\text{off}})) = 0 \quad (7)$$

Proof. See Appendix A. \square

According to Proposition 2, the resampling method is asymptotically equivalent to the reweighting method and can also deconfound the offline data provided that the offline dataset is large enough.

The advantages of the above two deconfounding methods are obvious. On the one hand, since both the reweighting and resampling methods decouple the deconfounding process from the RL algorithm, these methods can be easily combined

with existing offline RL algorithms provided that the weak condition in Assumption 1 is satisfied. On the other hand, the implementation of these methods is quite straightforward, only requiring minor modification to the original RL algorithms, i.e., we only need to incorporate the estimated $d_1(\tau)$ into the loss function.

3.3 Simplification of the Causal Models

The convergence rate of conditional density estimation (CDE) decreases exponentially as the dimension of the variables increases due to the curse of dimensionality. Therefore, it is necessary to simplify the causal models by reducing the dimensions of the variables in the process of CDE, so that our deconfounding methods can be applied to problems with higher-dimensional variables. For example, if the confounder exists only between the action and reward, we can simplify the causal model correspondingly by ignoring the variable s' in the process of CDE. We formally define two types of simplified causal models for two specific cases and derive the corresponding simplified forms of $d_1(\tau)$ in Appendix D.

4 Results

Evaluation of the deconfounding method is a challenging issue due to the lack of benchmark tasks. In addition, there is little work in deep RL on learning from observational data with confounders. To this end, we design four benchmark tasks, namely, EmotionalPendulum, WindyPendulum, EmotionalPendulum*, and WindyPendulum*, by modifying the Pendulum task in the OpenAI Gym [Brockman *et al.*, 2016]. All the implementations of the offline RL algorithms in this paper follow d3rlpy, an offline RL library [Takuma Seno, 2021]. All the hyperparameters of the offline RL algorithms are set to the default values of d3rlpy. The rewards are tested over 20 episodes every 1000 learning steps, and averaged over 5 random seeds. Other hyperparameters and the implementation details are described in Appendix C.

4.1 Unobserved Confounders

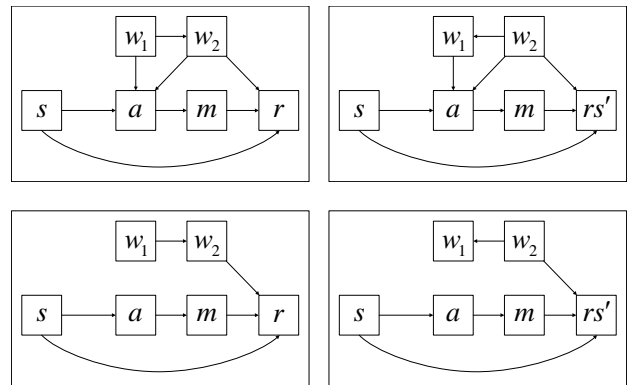


Figure 3: **Left:** the causal graphs depicting the offline and online data generating processes in EmotionalPendulum. **Right:** the causal graphs depicting the offline and online data generating processes in WindyPendulum. In both tasks, the confounders in the offline data are unobserved.

Figure 3 shows the graphical models for EmotionalPendulum and WindyPendulum, where the confounders are unobserved in the offline data. Obviously, these graphical models are special cases of the graphical models described in Section 2. In both tasks, we assume that there is an entertainment facility similar to a pendulum. One end of the pendulum is attached to a fixed point and a human sitting in a seat at the other end of the pendulum needs to swing the pendulum to an upright position. However, the controller of the pendulum fails intermittently, i.e., the action $a \in \{-2, -1, 0, 1, 2\}$ that the human wants to take may not equal the actual action $m \in \{-2, -1, 0, 1, 2\}$ executed by the machine. Specifically, in most cases, m is equal to a , and there is a probability p_{fail} that m randomly selects an action in the action space, with each action equally likely to be selected. There are some sensors are used to collect the confounded offline data generated in the above human-environment interaction process. Note that the environmental information o_2 in these offline data includes the state s and the actual action m executed by the machine. The offline RL algorithms need to use these confounded offline data to train an agent that substitutes the human to control the pendulum in the testing environment, where the confounders are unobserved, i.e., $o_3 = \{s\}$. The main difference between the two tasks is that the confounders in EmotionalPendulum are between the action and reward while the confounders in WindyPendulum are between the action, reward and next state.

The design of EmotionalPendulum refers to the real-world phenomenon that humans may take some actions that are not rational when they are in negative emotions such as boredom and fear. Specifically, we assume that the human sitting in the entertainment facility may feel afraid and decide to slow down if the speed is too fast (i.e., if the speed $|v|$ is above the threshold v_T), or feel boring and decide to speed up if the speed is too slow (i.e., if $|v| \leq v_T$), and will make rational decisions according to the trained agent if the emotions of the human are not negative, i.e., the behavior policy of the human depends on $o_1 = \{s, w_1, w_2\}$, where w_1 denotes whether the human has negative emotions and w_2 denotes whether the expressions of the human are negative. Then, the environment will return a reward $r = r_o + r_a$, where r_o denotes the original reward in the Pendulum task and r_a denotes an additional reward that is generated by the environment to encourage the human if the emotions are negative.

In WindyPendulum, we take into consideration the wind that may change the direction arbitrarily at each step. We assume that the wind force is 2.5 times larger than the largest force applied to the pendulum by the human/agent and the human will feel afraid if there is a strong wind. The human in a state of fear may choose the force opposite to the wind or decide to slow down, or choose the rational action, i.e., the behavior policy of the human depends on $o_1 = \{s, w_1, w_2\}$, where w_1 denotes whether the human is afraid due to the wind and w_2 denotes the direction of the wind. See Appendix E for more details of the description of the two tasks. Similar to EmotionalPendulum, a reward $r = r_o + r_a$ is then received, where the additional reward r_a is used to encourage the human if the wind exists.

As shown in Figure 4, we compare the deep RL algorithms

p_{fail}	$odds_1$	v_T	$I_{p,1}$	BC	CQL	CQL_RW	CQL_RS
0.2	4	0.5	0.7	-1020.0	-236.3	114.4	153.9
		0.9	0.9	-1145.9	-552.5	59.1	100.6
		1.0	0.7	-857.6	-98.5	180.1	181.8
	6	0.5	0.9	-1096.5	-531.5	85.2	113.6
		0.9	0.7	-361.2	46.3	92.4	84.6
		1.0	0.9	-999.2	-70.7	36.8	72.3
0.1	4	0.5	0.7	-399.9	77.9	93.3	95.1
		0.9	0.9	-834.5	-25.6	83.3	76.9
		1.0	0.9	-977.2	-82.0	115.0	123.1
	6	0.5	0.7	-1126.7	-523.1	97.2	44.5
		0.9	0.9	-884.7	81.7	206.5	225.2
		1.0	0.9	-1065.8	-443.5	56.3	144.3

Table 2: Comparison of BC, CQL, CQL_RW, and CQL_RS under different settings of EmotionalPendulum.

DQN, DDQN, SAC and CQL with and without our deconfounding methods in EmotionalPendulum and WindyPendulum, respectively. DQN_RW denotes the DQN algorithm that uses the reweighting method and DQN_RS for the resampling method. Other algorithms are denoted similarly. It is clear that the deconfounding deep RL algorithms perform better than the original deep RL algorithms in both tasks.

We take EmotionalPendulum as an example to specifically illustrate the confounding problem and why our proposed methods could perform better than the original deep RL algorithms. As shown in the top left of Figure 3, the association flowing along the directed path $a \rightarrow m \rightarrow r$ is causal association, while the association flowing along $a \leftarrow w_1 \rightarrow w_2 \rightarrow r$ is non-causal association. In other words, because the human may take irrational actions when he/she is in negative emotions, and because the environment may return some additional reward if the emotions of the human are negative, there is non-causal association between the irrational action and the additional reward, which may mislead the human to believe that the irrational action will be well rewarded. Given s , there is only causal association between a and r in the online data, because the non-causal association flowing along $a \leftarrow s \rightarrow r$ is blocked by s . In contrast, given s , there are both causal association and non-causal association between a and r in the offline data. Therefore, the original deep RL algorithms trained using confounded offline data will be misled by non-causal association in the data, and thus perform poorly in the online environment. However, the deconfounding deep RL algorithms can learn causal association from confounded offline data, and thus perform well in the online environment.

So, what will happen if we enhance the non-causal association flowing along $a \leftarrow w_1 \rightarrow w_2 \rightarrow r$ in the offline data? The values of the environmental hyperparameters of EmotionalPendulum, which correspond to the top row of Figure 4, are as follows: $p_{fail} = 0.2$, $odds_1 = 4$, $v_T = 1$, and $I_{p,1} = 0.7$, where $I_{p,1}$ denotes the probability of the human choosing irrational actions when he/she has negative emotions and $odds_1$ denotes the odds that the human does not have negative emotions. Clearly, if we keep the other hyperparameters constant and increase the value of

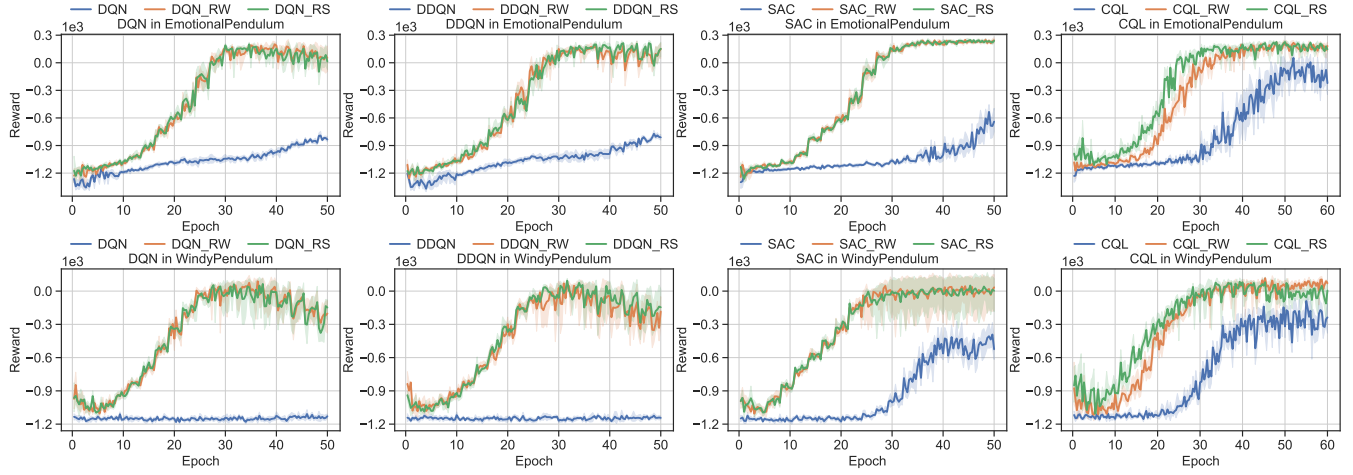


Figure 4: Performance of the deep RL algorithms with and without our deconfounding methods in EmotionalPendulum and WindyPendulum.

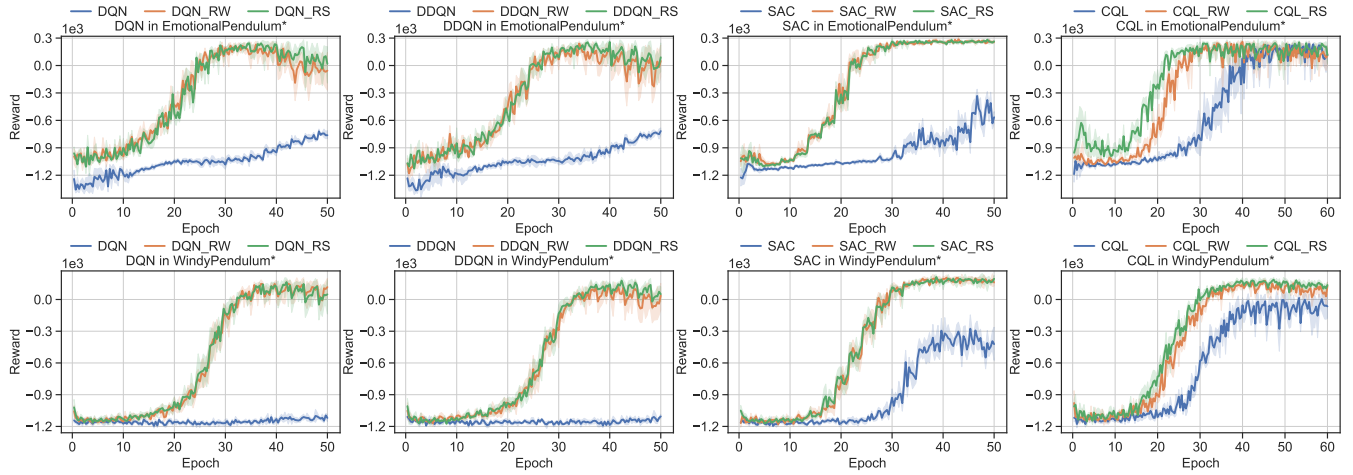


Figure 5: Performance of the deep RL algorithms with and without our deconfounding methods in EmotionalPendulum* and WindyPendulum*.

$I_{p,1}$ from 0.7 to 0.9, the non-causal association flowing along $a \leftarrow w_1 \rightarrow w_2 \rightarrow r$ in the offline data will be enhanced. As shown in Table 2, the enhancement of the non-causal association leads to increases in the gaps between the performance of CQL and CQL.RW, and between the performance of CQL and CQL.RS. Additionally, Table 2 shows that, no matter how much p_{fail} , $odds_1$, and v_T are, the gaps increase if we increase the value of $I_{p,1}$ from 0.7 to 0.9. Similarly, if we keep the other hyperparameters constant, reducing the value of $odds_1$ leads to an enhancement of the non-causal association. As shown in Table 2, regardless of how much p_{fail} , v_T , and $I_{p,1}$ are, the gaps increase if we reduce the value of $odds_1$ from 6 to 4.

Moreover, CQL.RW and CQL.RS perform better than CQL under all settings in Table 2, which verifies the robustness of our deconfounding methods. In addition, as shown in Table 2, the behavior cloning (BC) algorithm performs much worse than CQL, CQL.RW and CQL.RS because the

offline data are not expert data. In both EmotionalPendulum and WindyPendulum, the behavior policy of the human performs poorly, because the human takes many irrational actions based on his/her emotions. Therefore, imitation learning methods such as BC are not suitable for both tasks. In fact, in addition to Table 2, we compare BC, the original deep RL algorithms, and the deconfounding deep RL algorithms under different settings in Appendix E to verify the robustness of our deconfounding methods. Furthermore, we perform some ablation experiments in Appendix E.

4.2 Partially Observed Confounders

In the above two tasks, we assume that the confounders in the offline data are unobserved and identify the causal effect based on a variation of the frontdoor criterion. By contrast, in the two new tasks, EmotionalPendulum* and WindyPendulum*, we assume that the confounders in the offline data are partially observed and condition on a subset of the confounders to identify the causal effect. In the new tasks, the

controller of the pendulum never fails, i.e., the action a that the human wants to take is the same as the actual action m executed by the machine. The corresponding causal graphs and details of these two new tasks are given in Appendix E. To solve the new tasks, we define a new CMDP and two new SCMs and derive two new deconfounding methods under the new definitions in Appendix B. As shown in Figure 5, the deconfounding deep RL algorithms perform better than the original deep RL algorithms. Additionally, in Appendix E, we compare BC, the original deep RL algorithms, and the deconfounding deep RL algorithms under different settings.

5 Related Work

A number of studies [Lattimore *et al.*, 2016; Nair and Jiang, 2021] seek to introduce causality into the field of RL in various settings, where the use of observational data [Wang *et al.*, 2021; Lu *et al.*, 2018; Gasse *et al.*, 2021] is one of the key issues.

The Bandit Problem. The Causal bandit problem [Lattimore *et al.*, 2016] seeks to learn the optimal intervention from the interventional data, which conform to a causal graph, to minimise a simple regret. Sen *et al.* [2017] propose the successive rejects algorithms and derive the gap-dependent bounds for causal bandit based on importance sampling. The Contextual bandit problem [Langford and Zhang, 2007] seeks to learn a policy which depends on the context, namely the environmental variables, to maximize the reward which depends on the action and the context. Kallus and Zhou [2018] propose algorithms for OPE and learning from the confounded observational data with continuous actions based on the inverse probability weighting. Our paper, however, studies the causal RL problem which is more difficult than the bandit problem with a longer horizon.

Causal RL. There is some work studying causal RL in the model-based RL settings. Lu *et al.* [2018] propose a model-based RL method that estimates an SCM from observational data with the time-invariant confounder between the action and reward based on the latent-variable model proposed by Louizos *et al.* [2017]. This model, however, cannot estimate the correct causal effect provided that the latent variable is misspecified or the data distribution is complex as shown by Rissanen and Marttinen [2021]. Gasse *et al.* [2021] combine interventional data with observational data to estimate the latent-based transition model, which can be used for model-based RL. However, since that the time consumed by their program increases rapidly as the size of the discrete latent space increases, and that they assume that the state space is smaller than the discrete latent space, their algorithm can only be used to address problems with small state spaces. On the contrary, our deconfounding methods can be applied to problems with both continuous and discrete variables and our assumptions do not restrict the size of the state and confounder spaces. The closest work is the one by Wang *et al.* [2021], where the authors focus on how to improve the sample efficiency of the online algorithm by incorporating large amounts of observational data in the model-free RL settings. However, they follow the assumption of Yang and Wang [2019; 2020]; Jin *et al.* [2020] that the transition kernels and reward

functions are linear, so that the corresponding SCMs are also linear [Peters *et al.*, 2017]. This strong assumption is hard to hold in the real world, where the dynamics of the environment are nonlinear. Furthermore, they assume that there is very complex correlation between the backdoor-adjusted or frontdoor-adjusted feature and another feature. For example, they assume that the backdoor-adjusted feature is the expectation of the state-action-confounder feature. These assumptions make their theoretical algorithms difficult to implement. In contrast, the transition kernels and reward functions in our assumptions can be nonlinear, and experiments are provided to verify the performance of the offline RL algorithms combined with our deconfounding methods.

Off-Policy Evaluation. A line of work in the OPE field uses confounded data to estimate the performance of the evaluation policy. There are several papers that design estimators for the partially observable Markov decision process in the tabular setting [Nair and Jiang, 2021; Tennenholz *et al.*, 2020], which cannot be applied to the large or continuous state space. Recently a lot of work [Kallus and Zhou, 2020; Gelada and Bellemare, 2019; Hallak and Mannor, 2017; Kallus and Uehara, 2019; Liu *et al.*, 2018] proposes algorithms for OPE based on the importance sampling technique. However, these algorithms estimate the stationary distribution density ratio, which changes as the evaluation policy changes. This makes their work inapplicable to the RL field, where the evaluation policy is always changing. Instead, since we realize that SAC, DQN, and other off-policy RL algorithms utilize only the single-step transition in the data, our deconfounding methods are based on the conditional distribution density ratio, which remains constant in the learning process, so that our work can be applied to the RL field.

6 Conclusion

In this paper, we propose two plug-in deconfounding methods based on the importance sampling and causal inference techniques for model-free deep RL algorithms. These two methods can be applied to large and continuous environments. In addition, we prove that our deconfounding methods can construct an unbiased loss function w.r.t the online data and show that the deconfounding deep RL algorithms perform better than the original deep RL algorithms in the four benchmark tasks which are created by modifying the OpenAI Gym. A limitation of our work is the assumption that we already know the causal graph of the environment. In future work, we plan to build a causal model through causal discovery without prior knowledge of the environment and to deconfound the confounded data based on the discovered causal model. We hope that our deconfounding methods can bridge the gap between offline RL algorithms and real-world problems by leveraging large amounts of observational data.

Acknowledgments

This work is supported in part by the National Key Research and Development Program of China (No. 2021ZD0112400), the NSFC-Liaoning Province United Foundation under Grant U1908214, the National Natural Science Foundation of China

(No. 62076259), the 111 Project (No. D23006), the Fundamental Research Funds for the Central Universities under grant DUT21TD107, DUT22ZD214, the LiaoNing Revitalization Talents Program (No. XLYC2008017), the Fundamental and Application Research Funds of Guangdong province (No. 2023A1515012946), and the Fundamental Research Funds for the Central Universities-Sun Yat-sen University. The authors would like to thank Zifan Wu for revising the author response to the reviewers.

References

[Agarwal *et al.*, 2020] Rishabh Agarwal, Dale Schuurmans, and Mohammad Norouzi. An optimistic perspective on offline reinforcement learning. In *International Conference on Machine Learning*, pages 104–114. PMLR, 2020.

[Brockman *et al.*, 2016] Greg Brockman, Vicki Cheung, Ludwig Pettersson, Jonas Schneider, John Schulman, Jie Tang, and Wojciech Zaremba. Openai gym. *arXiv preprint arXiv:1606.01540*, 2016.

[Ernst *et al.*, 2005] Damien Ernst, Pierre Geurts, and Louis Wehenkel. Tree-based batch mode reinforcement learning. *Journal of Machine Learning Research*, 6:503–556, 2005.

[Fujimoto *et al.*, 2019] Scott Fujimoto, David Meger, and Doina Precup. Off-policy deep reinforcement learning without exploration. In *International Conference on Machine Learning*, pages 2052–2062. PMLR, 2019.

[Gasse *et al.*, 2021] Maxime Gasse, Damien Grasset, Guillaume Gaudron, and Pierre-Yves Oudeyer. Causal reinforcement learning using observational and interventional data. *arXiv preprint arXiv:2106.14421*, 2021.

[Gelada and Bellemare, 2019] Carles Gelada and Marc G Bellemare. Off-policy deep reinforcement learning by bootstrapping the covariate shift. In *Proceedings of the AAAI Conference on Artificial Intelligence*, volume 33, pages 3647–3655, 2019.

[Glymour *et al.*, 2016] Madelyn Glymour, Judea Pearl, and Nicholas P Jewell. *Causal inference in statistics: A primer*. John Wiley & Sons, 2016.

[Haarnoja *et al.*, 2017] Tuomas Haarnoja, Haoran Tang, Pieter Abbeel, and Sergey Levine. Reinforcement learning with deep energy-based policies. In *International Conference on Machine Learning*, pages 1352–1361. PMLR, 2017.

[Hallak and Mannor, 2017] Assaf Hallak and Shie Mannor. Consistent on-line off-policy evaluation. In *International Conference on Machine Learning*, pages 1372–1383. PMLR, 2017.

[Jaques *et al.*, 2019] Natasha Jaques, Asma Ghandeharioun, Judy Hanwen Shen, Craig Ferguson, Agata Lapedriza, Noah Jones, Shixiang Gu, and Rosalind Picard. Way off-policy batch deep reinforcement learning of implicit human preferences in dialog. *arXiv preprint arXiv:1907.00456*, 2019.

[Jin *et al.*, 2020] Chi Jin, Zhuoran Yang, Zhaoran Wang, and Michael I Jordan. Provably efficient reinforcement learning with linear function approximation. In *Conference on Learning Theory*, pages 2137–2143. PMLR, 2020.

[Kallus and Uehara, 2019] Nathan Kallus and Masatoshi Uehara. Efficiently breaking the curse of horizon in off-policy evaluation with double reinforcement learning. *arXiv preprint arXiv:1909.05850*, 2019.

[Kallus and Zhou, 2018] Nathan Kallus and Angela Zhou. Policy evaluation and optimization with continuous treatments. In *International conference on artificial intelligence and statistics*, pages 1243–1251. PMLR, 2018.

[Kallus and Zhou, 2020] Nathan Kallus and Angela Zhou. Confounding-robust policy evaluation in infinite-horizon reinforcement learning. *arXiv preprint arXiv:2002.04518*, 2020.

[Kumar *et al.*, 2019] Aviral Kumar, Justin Fu, George Tucker, and Sergey Levine. Stabilizing off-policy q-learning via bootstrapping error reduction. *arXiv preprint arXiv:1906.00949*, 2019.

[Kumar *et al.*, 2020] Aviral Kumar, Aurick Zhou, George Tucker, and Sergey Levine. Conservative q-learning for offline reinforcement learning. *arXiv preprint arXiv:2006.04779*, 2020.

[Langford and Zhang, 2007] John Langford and Tong Zhang. The epoch-greedy algorithm for multi-armed bandits with side information. In J. Platt, D. Koller, Y. Singer, and S. Roweis, editors, *Advances in Neural Information Processing Systems*, volume 20. Curran Associates, Inc., 2007.

[Lattimore *et al.*, 2016] Finnian Lattimore, Tor Lattimore, and Mark D Reid. Causal bandits: Learning good interventions via causal inference. *arXiv preprint arXiv:1606.03203*, 2016.

[Levine *et al.*, 2020] Sergey Levine, Aviral Kumar, George Tucker, and Justin Fu. Offline reinforcement learning: Tutorial, review, and perspectives on open problems. *arXiv preprint arXiv:2005.01643*, 2020.

[Liu *et al.*, 2018] Qiang Liu, Lihong Li, Ziyang Tang, and Dengyong Zhou. Breaking the curse of horizon: Infinite-horizon off-policy estimation. *arXiv preprint arXiv:1810.12429*, 2018.

[Lloyd, 1982] Stuart Lloyd. Least squares quantization in pcm. *IEEE transactions on information theory*, 28(2):129–137, 1982.

[Louizos *et al.*, 2017] Christos Louizos, Uri Shalit, Joris M Mooij, David Sontag, Richard Zemel, and Max Welling. Causal effect inference with deep latent-variable models. In I. Guyon, U. Von Luxburg, S. Bengio, H. Wallach, R. Fergus, S. Vishwanathan, and R. Garnett, editors, *Advances in Neural Information Processing Systems*, volume 30. Curran Associates, Inc., 2017.

[Lu *et al.*, 2018] Chaochao Lu, Bernhard Schölkopf, and José Miguel Hernández-Lobato. Deconfounding re-

inforcement learning in observational settings. *arXiv preprint arXiv:1812.10576*, 2018.

[MacQueen, 1967] J MacQueen. Classification and analysis of multivariate observations. In *5th Berkeley Symp. Math. Statist. Probability*, pages 281–297. University of California Los Angeles LA USA, 1967.

[Mnih *et al.*, 2013] Volodymyr Mnih, Koray Kavukcuoglu, David Silver, Alex Graves, Ioannis Antonoglou, Daan Wierstra, and Martin Riedmiller. Playing atari with deep reinforcement learning. *arXiv preprint arXiv:1312.5602*, 2013.

[Nagler, 2018] Thomas Nagler. A generic approach to non-parametric function estimation with mixed data. *Statistics & Probability Letters*, 137:326–330, 2018.

[Nair and Jiang, 2021] Yash Nair and Nan Jiang. A spectral approach to off-policy evaluation for pomdps. *arXiv preprint arXiv:2109.10502*, 2021.

[Pearl, 2009] Judea Pearl. *Causality*. Cambridge university press, 2009.

[Pearl, 2012] Judea Pearl. The do-calculus revisited. *arXiv preprint arXiv:1210.4852*, 2012.

[Peters *et al.*, 2017] Jonas Peters, Dominik Janzing, and Bernhard Schölkopf. *Elements of causal inference: foundations and learning algorithms*. The MIT Press, 2017.

[Rissanen and Marttinen, 2021] Severi Rissanen and Pekka Marttinen. A critical look at the consistency of causal estimation with deep latent variable models. In M. Ranzato, A. Beygelzimer, Y. Dauphin, P.S. Liang, and J. Wortman Vaughan, editors, *Advances in Neural Information Processing Systems*, volume 34, pages 4207–4217. Curran Associates, Inc., 2021.

[Rothfuss *et al.*, 2019] Jonas Rothfuss, Fabio Ferreira, Simon Walther, and Maxim Ulrich. Conditional density estimation with neural networks: Best practices and benchmarks. *arXiv:1903.00954*, 2019.

[Sen *et al.*, 2017] Rajat Sen, Karthikeyan Shanmugam, Alexandros G Dimakis, and Sanjay Shakkottai. Identifying best interventions through online importance sampling. In *International Conference on Machine Learning*, pages 3057–3066. PMLR, 2017.

[Siegel *et al.*, 2020] Noah Y Siegel, Jost Tobias Springenberg, Felix Berkenkamp, Abbas Abdolmaleki, Michael Neunert, Thomas Lampe, Roland Hafner, Nicolas Heess, and Martin Riedmiller. Keep doing what worked: Behavioral modelling priors for offline reinforcement learning. *arXiv preprint arXiv:2002.08396*, 2020.

[Sugiyama *et al.*, 2010] Masashi Sugiyama, Ichiro Takeuchi, Taiji Suzuki, Takafumi Kanamori, Hirotaka Hachiya, and Daisuke Okanohara. Conditional density estimation via least-squares density ratio estimation. In Yee Whye Teh and Mike Titterington, editors, *Proceedings of the Thirteenth International Conference on Artificial Intelligence and Statistics*, volume 9 of *Proceedings of Machine Learning Research*, pages 781–788, Chia Laguna Resort, Sardinia, Italy, 13–15 May 2010. PMLR.

[Sutton and Barto, 2018] Richard S Sutton and Andrew G Barto. *Reinforcement learning: An introduction*. MIT press, 2018.

[Takuma Seno, 2021] Michita Imai Takuma Seno. d3rlpy: An offline deep reinforcement library. In *NeurIPS 2021 Offline Reinforcement Learning Workshop*, December 2021.

[Tennenholz *et al.*, 2020] Guy Tennenholz, Uri Shalit, and Shie Mannor. Off-policy evaluation in partially observable environments. In *Proceedings of the AAAI Conference on Artificial Intelligence*, volume 34, pages 10276–10283, 2020.

[van Hasselt *et al.*, 2016] Hado van Hasselt, Arthur Guez, and David Silver. Deep reinforcement learning with double q-learning. In Dale Schuurmans and Michael P. Wellman, editors, *Proceedings of the Thirtieth AAAI Conference on Artificial Intelligence, February 12-17, 2016, Phoenix, Arizona, USA*, pages 2094–2100. AAAI Press, 2016.

[Wang *et al.*, 2021] Lingxiao Wang, Zhuoran Yang, and Zhaoran Wang. Provably efficient causal reinforcement learning with confounded observational data. In M. Ranzato, A. Beygelzimer, Y. Dauphin, P.S. Liang, and J. Wortman Vaughan, editors, *Advances in Neural Information Processing Systems*, volume 34, pages 21164–21175. Curran Associates, Inc., 2021.

[Yang and Wang, 2019] Lin Yang and Mengdi Wang. Sample-optimal parametric q-learning using linearly additive features. In *International Conference on Machine Learning*, pages 6995–7004. PMLR, 2019.

[Yang and Wang, 2020] Lin Yang and Mengdi Wang. Reinforcement learning in feature space: Matrix bandit, kernels, and regret bound. In *International Conference on Machine Learning*, pages 10746–10756. PMLR, 2020.

Causal Deep Reinforcement Learning using Observational Data

Appendix

A Mathematical Details

A.1 Difference between the Dynamics in the Offline Data and the Online Data

In Section 3, we claim that the dynamics are different between offline data and online data. Now we prove it formally.

Proof. From the law of total probability and the criterion for the identification of covariate-specific effects, which is indicated by the Rule 2 in Chapter 3 of [Glymour *et al.*, 2016], we obtain:

$$\hat{P}(s', r|s, a) = \sum_w \hat{P}(s', r|a, w, s) \hat{P}(w|s, a) \quad (8)$$

and

$$\begin{aligned} \bar{P}(s', r|s, a) &= \hat{P}(s', r|s, do(a)) \\ &= \sum_w \hat{P}(s', r|a, w, s) \hat{P}(w|s). \end{aligned} \quad (9)$$

Since a depends on w given s in the offline data, $\hat{P}(w|s, a) \neq \hat{P}(w|s)$. Therefore the above two are different. \square

A.2 Proof of Proposition 1

Proposition. *Under the definitions of the CMDP and SCMs in Section 2, it holds that*

$$\begin{aligned} L_2(\phi, \mathcal{D}_{\text{off}}) &\triangleq \mathbb{E}_{s, a \sim \mathcal{D}_{\text{off}}} [\mathbb{E}_{s', r \sim \bar{P}(\cdot, \cdot|s, a)} [f_\phi + h_\phi]] \\ &= \mathbb{E}_{s, a \sim \mathcal{D}_{\text{off}}} [\mathbb{E}_{s', r, m \sim \hat{P}(\cdot, \cdot, \cdot|s, a)} [d_1(s, m, a, s', r) f_\phi + h_\phi]] \\ &= \mathbb{E}_{s, a, s', r, m \sim \mathcal{D}_{\text{off}}} [d_1(s, m, a, s', r) f_\phi + h_\phi] \end{aligned} \quad (10)$$

Proof. From the importance sampling, we obtain:

$$\begin{aligned} L_2(\phi, \mathcal{D}_{\text{off}}) &\triangleq \mathbb{E}_{s, a \sim \mathcal{D}_{\text{off}}} [\mathbb{E}_{s', r \sim \bar{P}(\cdot, \cdot|s, a)} [f_\phi + h_\phi]] \\ &= \mathbb{E}_{s, a \sim \mathcal{D}_{\text{off}}} \left[\mathbb{E}_{s', r, m \sim \hat{P}(\cdot, \cdot, \cdot|s, a)} \left[\frac{\bar{P}(s', r, m|s, a)}{\hat{P}(s', r, m|s, a)} f_\phi \right] + h_\phi \right] \\ &= \mathbb{E}_{s, a, s', r, m \sim \mathcal{D}_{\text{off}}} \left[\frac{\bar{P}(s', r, m|s, a)}{\hat{P}(s', r, m|s, a)} f_\phi + h_\phi \right]. \end{aligned}$$

According to do-calculus, we obtain:

$$\begin{aligned} \frac{\bar{P}(s', r, m|s, a)}{\hat{P}(s', r, m|s, a)} &= \frac{\hat{P}(s', r, m|s, do(a))}{\hat{P}(s', r, m|s, a)} \\ &= \frac{\hat{P}(s', r|m, s, do(a)) \hat{P}(m|s, do(a))}{\hat{P}(s', r|m, s, a) \hat{P}(m|s, a)}. \end{aligned}$$

According to do-calculus, we obtain: $\hat{P}(m|s, do(a)) = \hat{P}(m|s, a)$, and

$$\begin{aligned} \hat{P}(s', r|m, s, do(a)) &= \hat{P}(s', r|s, do(m), do(a)) \\ &= \hat{P}(s', r|s, do(m)) \\ &= \sum_{a'} \hat{P}(s', r|m, a', s) \hat{P}(a'|s). \end{aligned}$$

By bringing in the two equations, we obtain:

$$\frac{\bar{P}(s', r, m|s, a)}{\hat{P}(s', r, m|s, a)} = \frac{\sum_{a'} \hat{P}(s', r|m, a', s) \hat{P}(a'|s)}{\hat{P}(s', r|m, s, a)}.$$

By bringing in this equation, we obtain:

$$L_2(\phi, \mathcal{D}_{\text{off}}) = \mathbb{E}_{s,a,s',r,m \sim \mathcal{D}_{\text{off}}} \left[\frac{\sum_{a'} \hat{P}(s', r|m, a', s) \hat{P}(a'|s)}{\hat{P}(s', r|m, a, s)} f_\phi + h_\phi \right].$$

□

A.3 Proof of Proposition 2

Proposition. *Under the definitions of the CMDP and SCMs in Section 2, the loss function of the resampling method is asymptotically equal to that of the reweighting method as in Equation 11 provided that the dataset is large enough.*

$$\lim_{N \rightarrow \infty} (L_3(\phi, \mathcal{D}_{\text{off}}) - L_2(\phi, \mathcal{D}_{\text{off}})) = 0 \quad (11)$$

Proof. Slightly modifying the first step of the proof in Appendix A.2, we obtain:

$$\begin{aligned} L_2(\phi, \mathcal{D}_{\text{off}}) &\triangleq \mathbb{E}_{s,a \sim \mathcal{D}_{\text{off}}} [\mathbb{E}_{s',r \sim \bar{P}(\cdot,\cdot|s,a)} [f_\phi + h_\phi]] \\ &= \mathbb{E}_{s,a \sim \mathcal{D}_{\text{off}}} \left[\mathbb{E}_{s',r,m \sim \hat{P}(\cdot,\cdot|s,a)} \left[\frac{\bar{P}(s',r,m|s,a)}{\hat{P}(s',r,m|s,a)} (f_\phi + h_\phi) \right] \right] \\ &= \mathbb{E}_{s,a,s',r,m \sim \mathcal{D}_{\text{off}}} [d_1(s, m, a, s', r) (f_\phi + h_\phi)]. \end{aligned}$$

Then, based on the reparameterization trick, we obtain:

$$L_2(\phi, \mathcal{D}_{\text{off}}) = \mathbb{E}_{I \sim \text{DiscreteU}(1,N)} [d_{1,I}(f_\phi(s_I, a_I, s'_I, r_I) + h_\phi(s_I, a_I))],$$

where $\text{DiscreteU}(1, N)$ denotes the discrete uniform distribution on the integers $1, 2, \dots, N$.

Furthermore, from the importance sampling, we obtain:

$$L_2(\phi, \mathcal{D}_{\text{off}}) = \mathbb{E}_{I \sim p_1} \left[\frac{\frac{1}{N}}{p_1(I)} d_{1,I}(f_\phi(s_I, a_I, s'_I, r_I) + h_\phi(s_I, a_I)) \right].$$

And then, the formula can be simplified to

$$\begin{aligned} L_2(\phi, \mathcal{D}_{\text{off}}) &= \mathbb{E}_{I \sim p_1} \left[\frac{\sum_{j=1}^N d_{1,j}}{N} (f_\phi(s_I, a_I, s'_I, r_I) + h_\phi(s_I, a_I)) \right] \\ &= L_3(\phi, \mathcal{D}_{\text{off}}) \frac{\sum_{j=1}^N d_{1,j}}{N}. \end{aligned}$$

Thus,

$$\lim_{N \rightarrow \infty} (L_3(\phi, \mathcal{D}_{\text{off}}) - L_2(\phi, \mathcal{D}_{\text{off}})) = \lim_{N \rightarrow \infty} L_3(\phi, \mathcal{D}_{\text{off}}) \left(1 - \frac{\sum_{j=1}^N d_{1,j}}{N} \right).$$

Since

$$\begin{aligned} \lim_{N \rightarrow \infty} \left(1 - \frac{\sum_{j=1}^N d_{1,j}}{N} \right) &= 1 - \lim_{N \rightarrow \infty} \mathbb{E}_{I \sim \text{DiscreteU}(1,N)} [d_{1,I}] \\ &= 1 - \lim_{N \rightarrow \infty} \mathbb{E}_{s,a,s',r,m \sim \mathcal{D}_{\text{off}}} [d_1(s, m, a, s', r)] \\ &= 1 - \lim_{N \rightarrow \infty} \mathbb{E}_{s,a \sim \mathcal{D}_{\text{off}}} \left[\mathbb{E}_{s',r,m \sim \hat{P}(\cdot,\cdot|s,a)} \left[\frac{\bar{P}(s',r,m|s,a)}{\hat{P}(s',r,m|s,a)} \right] \right] \\ &= 1 - \lim_{N \rightarrow \infty} \mathbb{E}_{s,a \sim \mathcal{D}_{\text{off}}} [\mathbb{E}_{s',r,m \sim \bar{P}(\cdot,\cdot|s,a)} [1]] \\ &= 0, \end{aligned}$$

and the limit of the loss function of the neural network is finite, we obtain:

$$\lim_{N \rightarrow \infty} (L_3(\phi, \mathcal{D}_{\text{off}}) - L_2(\phi, \mathcal{D}_{\text{off}})) = \lim_{N \rightarrow \infty} L_3(\phi, \mathcal{D}_{\text{off}}) \lim_{N \rightarrow \infty} \left(1 - \frac{\sum_{j=1}^N d_{1,j}}{N} \right) = 0.$$

□

A.4 Proof of Proposition 3

Proposition. *Under Assumption 2 and the definitions of the CMDP and SCMs in Appendix B.1, it holds that*

$$\begin{aligned} L_2(\phi, \mathcal{D}_{\text{off}}) &\triangleq \mathbb{E}_{s,a \sim \mathcal{D}_{\text{off}}} [\mathbb{E}_{s',r \sim \bar{P}(\cdot,\cdot|s,a)} [f_\phi + h_\phi]] \\ &= \mathbb{E}_{s,a \sim \mathcal{D}_{\text{off}}} \left[\mathbb{E}_{s',r,u \sim \hat{P}(\cdot,\cdot,\cdot|s,a)} \left[\frac{\hat{P}(u|s)}{\hat{P}(u|s,a)} f_\phi + h_\phi \right] \right] \\ &= \mathbb{E}_{s,a,s',r,u \sim \mathcal{D}_{\text{off}}} \left[\frac{\hat{P}(u|s)}{\hat{P}(u|s,a)} f_\phi + h_\phi \right]. \end{aligned} \quad (12)$$

Proof. From the importance sampling, we obtain:

$$\begin{aligned} L_2(\phi, \mathcal{D}_{\text{off}}) &\triangleq \mathbb{E}_{s,a \sim \mathcal{D}_{\text{off}}} [\mathbb{E}_{s',r \sim \bar{P}(\cdot,\cdot|s,a)} [f_\phi + h_\phi]] \\ &= \mathbb{E}_{s,a \sim \mathcal{D}_{\text{off}}} \left[\mathbb{E}_{s',r,u \sim \hat{P}(\cdot,\cdot,\cdot|s,a)} \left[\frac{\bar{P}(s',r,u|s,a)}{\hat{P}(s',r,u|s,a)} f_\phi \right] + h_\phi \right] \\ &= \mathbb{E}_{s,a,s',r,u \sim \mathcal{D}_{\text{off}}} \left[\frac{\bar{P}(s',r,u|s,a)}{\hat{P}(s',r,u|s,a)} f_\phi + h_\phi \right]. \end{aligned}$$

Furthermore, based on do-calculus, we obtain:

$$\begin{aligned} L_2(\phi, \mathcal{D}_{\text{off}}) &= \mathbb{E}_{s,a,s',r,u \sim \mathcal{D}_{\text{off}}} \left[\frac{\hat{P}(s',r,u|s,do(a))}{\hat{P}(s',r,u|s,a)} f_\phi + h_\phi \right] \\ &= \mathbb{E}_{s,a,s',r,u \sim \mathcal{D}_{\text{off}}} \left[\frac{\hat{P}(s',r|u,s,do(a)) \hat{P}(u|s,do(a))}{\hat{P}(s',r|u,s,a) \hat{P}(u|s,a)} f_\phi + h_\phi \right]. \end{aligned}$$

According to do-calculus, we obtain:

$$\hat{P}(s',r|u,s,do(a)) = \hat{P}(s',r|u,s,a),$$

and

$$\hat{P}(u|s,do(a)) = \hat{P}(u|s).$$

By bringing in the two equations, we obtain:

$$L_2(\phi, \mathcal{D}_{\text{off}}) = \mathbb{E}_{s,a,s',r,u \sim \mathcal{D}_{\text{off}}} \left[\frac{\hat{P}(u|s)}{\hat{P}(u|s,a)} f_\phi + h_\phi \right].$$

□

A.5 Proof of Proposition 4

Proposition. *Under Assumption 2 and the definitions of the CMDP and SCMs in Appendix B.1, the loss function of the resampling method is asymptotically equal to that of the reweighting method as in Equation 13 provided that the dataset is large enough.*

$$\lim_{N \rightarrow \infty} (L_3(\phi, \mathcal{D}_{\text{off}}) - L_2(\phi, \mathcal{D}_{\text{off}})) = 0 \quad (13)$$

Proof. Slightly modifying the first step of the proof in Appendix A.4, we obtain:

$$\begin{aligned}
L_2(\phi, \mathcal{D}_{\text{off}}) &\triangleq \mathbb{E}_{s, a \sim \mathcal{D}_{\text{off}}} [\mathbb{E}_{s', r \sim \bar{\mathbb{P}}(\cdot, \cdot | s, a)} [f_\phi + h_\phi]] \\
&= \mathbb{E}_{s, a \sim \mathcal{D}_{\text{off}}} \left[\mathbb{E}_{s', r, u \sim \hat{\mathbb{P}}(\cdot, \cdot | s, a)} \left[\frac{\bar{\mathbb{P}}(s', r, u | s, a)}{\hat{\mathbb{P}}(s', r, u | s, a)} (f_\phi + h_\phi) \right] \right] \\
&= \mathbb{E}_{s, a, r, s', u \sim \mathcal{D}_{\text{off}}} \left[\frac{\hat{\mathbb{P}}(u | s)}{\hat{\mathbb{P}}(u | s, a)} (f_\phi + h_\phi) \right].
\end{aligned}$$

Then, based on the reparameterization trick, we obtain:

$$L_2(\phi, \mathcal{D}_{\text{off}}) = \mathbb{E}_{I \sim \text{DiscreteU}(1, N)} \left[\frac{\hat{\mathbb{P}}(u_I | s_I)}{\hat{\mathbb{P}}(u_I | s_I, a_I)} (f_\phi(s_I, a_I, s'_I, r_I) + h_\phi(s_I, a_I)) \right].$$

Furthermore, from the importance sampling, we obtain:

$$L_2(\phi, \mathcal{D}_{\text{off}}) = \mathbb{E}_{I \sim p_2} \left[\frac{\frac{1}{N}}{p_2(I)} \frac{\hat{\mathbb{P}}(u_I | s_I)}{\hat{\mathbb{P}}(u_I | s_I, a_I)} (f_\phi(s_I, a_I, s'_I, r_I) + h_\phi(s_I, a_I)) \right].$$

And then, the formula can be simplified to

$$\begin{aligned}
L_2(\phi, \mathcal{D}_{\text{off}}) &= \mathbb{E}_{I \sim p_2} \left[\frac{\sum_{j=1}^N \frac{\hat{\mathbb{P}}(u_j | s_j)}{\hat{\mathbb{P}}(u_j | s_j, a_j)}}{N} (f_\phi(s_I, a_I, s'_I, r_I) + h_\phi(s_I, a_I)) \right] \\
&= L_3(\phi, \mathcal{D}_{\text{off}}) \frac{\sum_{j=1}^N \frac{\hat{\mathbb{P}}(u_j | s_j)}{\hat{\mathbb{P}}(u_j | s_j, a_j)}}{N}.
\end{aligned}$$

Thus,

$$\lim_{N \rightarrow \infty} (L_3(\phi, \mathcal{D}_{\text{off}}) - L_2(\phi, \mathcal{D}_{\text{off}})) = \lim_{N \rightarrow \infty} L_3(\phi, \mathcal{D}_{\text{off}}) \left(1 - \frac{\sum_{j=1}^N \frac{\hat{\mathbb{P}}(u_j | s_j)}{\hat{\mathbb{P}}(u_j | s_j, a_j)}}{N} \right).$$

Since

$$\begin{aligned}
\lim_{N \rightarrow \infty} \left(1 - \frac{\sum_{j=1}^N \frac{\hat{\mathbb{P}}(u_j | s_j)}{\hat{\mathbb{P}}(u_j | s_j, a_j)}}{N} \right) &= 1 - \lim_{N \rightarrow \infty} \mathbb{E}_{I \sim \text{DiscreteU}(1, N)} \left[\frac{\hat{\mathbb{P}}(u_I | s_I)}{\hat{\mathbb{P}}(u_I | s_I, a_I)} \right] \\
&= 1 - \lim_{N \rightarrow \infty} \mathbb{E}_{s, a, s', r, u \sim \mathcal{D}_{\text{off}}} \left[\frac{\hat{\mathbb{P}}(u | s)}{\hat{\mathbb{P}}(u | s, a)} \right] \\
&= 1 - \lim_{N \rightarrow \infty} \mathbb{E}_{s, a \sim \mathcal{D}_{\text{off}}} \left[\mathbb{E}_{s', r, u \sim \hat{\mathbb{P}}(\cdot, \cdot | s, a)} \left[\frac{\bar{\mathbb{P}}(s', r, u | s, a)}{\hat{\mathbb{P}}(s', r, u | s, a)} \right] \right] \\
&= 1 - \lim_{N \rightarrow \infty} \mathbb{E}_{s, a \sim \mathcal{D}_{\text{off}}} [\mathbb{E}_{s', r, u \sim \bar{\mathbb{P}}(\cdot, \cdot | s, a)} [1]] \\
&= 0,
\end{aligned}$$

and the limit of the loss function of the neural network is finite, we obtain:

$$\begin{aligned}
\lim_{N \rightarrow \infty} (L_3(\phi, \mathcal{D}_{\text{off}}) - L_2(\phi, \mathcal{D}_{\text{off}})) &= \lim_{N \rightarrow \infty} L_3(\phi, \mathcal{D}_{\text{off}}) \lim_{N \rightarrow \infty} \left(1 - \frac{\sum_{j=1}^N \frac{\hat{\mathbb{P}}(u_j | s_j)}{\hat{\mathbb{P}}(u_j | s_j, a_j)}}{N} \right) \\
&= 0.
\end{aligned}$$

□

B Background and Algorithms for Partially Observed Confounders

In Section 3, two deconfounding methods are proposed for the RL tasks where the confounders in the offline data are unobserved. In contrast, in this section, we derive two new deconfounding methods for the new RL tasks where the confounders in the offline data are partially observed. Before proposing the deconfounding methods, a CMDP and two SCMs different from those in Section 2 are defined to describe the new RL tasks.

B.1 Background for Partially Observed Confounders

The CMDP for partially observed confounders can be denoted by a seven-tuple $\langle \mathcal{S}, \mathcal{A}, \mathcal{W}, \mathcal{R}, P_1, P_2, \mu_0 \rangle$, where \mathcal{S} denotes the state space, \mathcal{A} denotes the discrete action space, \mathcal{W} denotes the confounder space, \mathcal{R} denotes the reward space, $P_1(s', r|s, w, a)$ denotes the dynamics of this CMDP, $P_2(w|s)$ denotes the confounder transition distribution, and $\mu_0(s)$ denotes the initial state distribution.

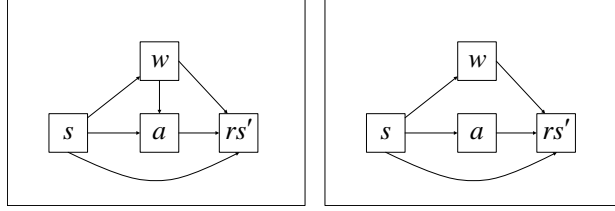


Figure 6: The left and right subfigures represent the SCM in the offline setting and online setting, respectively, which correspond to the CMDP for partially observed confounders. The behavior policy depends on w in the offline setting, but not in the online setting.

The SCM in the offline setting as shown in the first column of Figure 6 can be defined as a four-tuple $\langle U, V, F, P_e \rangle$, where the endogenous variables V includes (s, a, w, s', r) , and the set of structural functions F includes the state-reward transition distribution $P_1(s', r|s, w, a)$, the confounder transition distribution $P_2(w|s)$, and the behavior policy $\pi_b(a|s, w)$. The positivity assumption here is that, for $a \in \mathcal{A}, s \in \mathcal{S}, w \in \mathcal{W}$ such that $P(s, w) > 0, P(a|s, w) > 0$.

The SCM in the online setting where the agent can intervene on the variable a as shown in the second column of Figure 6 can be defined as another four-tuple $\langle U, V, F, P_e \rangle$, where the set of structural functions F includes the state-reward transition distribution $P_1(s', r|s, w, a)$, the confounder transition distribution $P_2(w|s)$, and the policy $\pi(a|s)$.

We assume that w is partially observable in the offline data, and condition on a subset u of w to identify the causal effect. Specifically, we assume that there exists an observable subset u of w such that $u \cup s$ satisfies the backdoor criterion, as in Assumption 2. Two examples are illustrated in Figure 7.

Assumption 2. Suppose there exists a set of observable variables $u \subseteq w$, such that $u \cup s$ satisfies: $u \cup s$ contains no descendant node of a and $u \cup s$ blocks every path between a and $s' \cup r$ that contains an arrow into a .

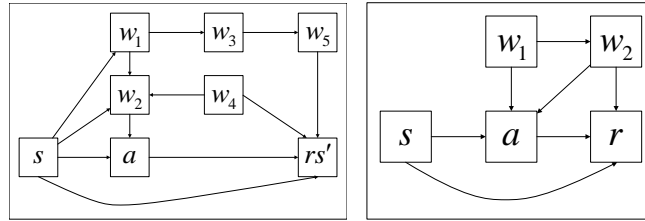


Figure 7: **Left:** $u = \{w_1, w_4\}$ satisfies the Assumption 2, which means that $u \cup s$ satisfies the backdoor criterion. **Right:** $u = \{w_2\}$ satisfies the Assumption 2, which means that $u \cup s$ satisfies the backdoor criterion.

B.2 Algorithms for Partially Observed Confounders

Under the definitions of the CMDP and SCMs in this section, two new deconfounding methods are proposed for the new RL tasks where the confounders in the offline data are partially observed. As shown in Figure 8, the new RL tasks are similar to the RL tasks where the confounders are unobserved in the offline data. Therefore, we only describe the differences between these tasks as follows. First, the intermediate state does not exist in the data generating process anymore. Second, the confounders are partially observed in the offline data, i.e., $o_2 = \{s, u\}$ where u satisfies Assumption 2.

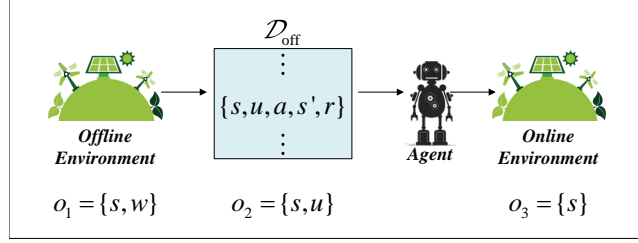


Figure 8: Diagram of the data flow framework, where the confounders in the offline data are partially observed.

Reweighting Method

Similar to Section 3, we incorporate an importance sampling ratio into the loss function based on importance sampling in the reweighting method. According to Proposition 3, the weighted loss function computed with offline data is unbiased, and the agent with this loss function can understand the environment correctly, while the original loss function as shown in Equation 14 is biased.

$$\begin{aligned} L_1(\phi, \mathcal{D}_{\text{off}}) &\triangleq \mathbb{E}_{s, a, s', r \sim \mathcal{D}_{\text{off}}} [f_\phi + h_\phi] \\ &= \mathbb{E}_{s, a \sim \mathcal{D}_{\text{off}}} \left[\mathbb{E}_{s', r \sim \hat{P}(\cdot, \cdot | s, a)} [f_\phi + h_\phi] \right] \end{aligned} \quad (14)$$

Proposition 3. *Under Assumption 2 and the definitions of the CMDP and SCMs in Appendix B.1, it holds that*

$$\begin{aligned} L_2(\phi, \mathcal{D}_{\text{off}}) &\triangleq \mathbb{E}_{s, a \sim \mathcal{D}_{\text{off}}} \left[\mathbb{E}_{s', r \sim \bar{P}(\cdot, \cdot | s, a)} [f_\phi + h_\phi] \right] \\ &= \mathbb{E}_{s, a \sim \mathcal{D}_{\text{off}}} \left[\mathbb{E}_{s', r, u \sim \hat{P}(\cdot, \cdot | s, a)} [d_2(u, s, a) f_\phi + h_\phi] \right] \\ &= \mathbb{E}_{s, a, s', r, u \sim \mathcal{D}_{\text{off}}} [d_2(u, s, a) f_\phi + h_\phi], \end{aligned} \quad (15)$$

where $d_2(u, s, a)$ is defined as follows:

$$d_2(u, s, a) = \frac{\hat{P}(u|s)}{\hat{P}(u|s, a)}. \quad (16)$$

Proof. See Appendix A.4. \square

Similar to Section 3, the new reweighting method can also be combined with existing model-free offline RL algorithms provided that Assumption 1 and Assumption 2 hold.

Resampling Method

Similar to Section 3, the resampling method extracts 5-tuples from the offline data with the unequal probabilities. However, due to the difference between SCMs, the probability of extracting elements from the offline data differs from Section 3. More specifically, the loss function for the offline RL algorithms with this resampling method is defined as follows:

$$L_3(\phi, \mathcal{D}_{\text{off}}) \triangleq \mathbb{E}_{I \sim p_2} [f_\phi(s_I, a_I, s'_I, r_I) + h_\phi(s_I, a_I)], \quad (17)$$

where $p_2(I = i) = d_{2,i} / \sum_{j=1}^N d_{2,j}$, $d_{2,i}$ is a shorthand for $\hat{P}(u_i|s_i)/\hat{P}(u_i|s_i, a_i)$, and s_i, a_i, r_i, s'_i, u_i denotes the state, action, reward, next state and observable set of the confounder in the i th 5-tuple of the offline dataset \mathcal{D}_{off} respectively. In this case, Proposition 4 holds.

Proposition 4. *Under Assumption 2 and the definitions of the CMDP and SCMs in Appendix B.1, the loss function of the resampling method is asymptotically equal to that of the reweighting method as in Equation 18 provided that the dataset is large enough.*

$$\lim_{N \rightarrow \infty} (L_3(\phi, \mathcal{D}_{\text{off}}) - L_2(\phi, \mathcal{D}_{\text{off}})) = 0 \quad (18)$$

Proof. See Appendix A.5. \square

According to Proposition 4, the new resampling method can also deconfound the offline data if the offline dataset is large enough. Additionally, the resampling method can also be applied to existing model-free offline RL algorithms provided that Assumption 1 and Assumption 2 hold.

C Implementation Details

Both the network architectures and optimizers are in the default settings of d3rlpy. In the process of estimating $d_1(\tau)$ and $d_2(u, s, a)$, we need to add noises to all discrete random variables. Specifically, we choose a noise $\epsilon_{\theta, v} = \epsilon + \theta(B_v - 0.5)$ where ϵ subjects to the uniform distribution $\mathcal{U}(-0.5, 0.5)$, B_v subjects to the beta distribution $\text{Beta}(v, v)$, $\theta = 0.5$ and $v = 5$. The task settings of Figure 4,5,12,13 are described in Table 3. Note that 1 epoch in Figure 4,5,10-15 represents 3000 learning steps. Other task settings and details of the four benchmark tasks are described in Appendix E.

EMOTIONALPENDULUM		
p_{fail}		0.2
v_T		1
$I_{p,1}$		0.7
$odds_1$		4
WINDYPENDULUM		
p_{fail}		0.1
$I_{p,2}$		0.9
$odds_2$		2.5
EMOTIONALPENDULUM*		
v_T		1
$I_{p,1}$		0.7
$odds_1$		4
WINDYPENDULUM*		
$I_{p,2}$		0.9
$odds_2$		2.5

Table 3: The task settings of Figure 4,5,12,13.

D Simplification of the Causal Models

In this section, CMDPs and SCMs for two specific cases of unobserved confounders are defined, and two corresponding simplified forms of $d_1(\tau)$ are derived.

D.1 The Confounder Exists Only between the Action and Reward

The CMDP for the first specific case of unobserved confounders can be denoted by a nine-tuple $\langle \mathcal{S}, \mathcal{M}, \mathcal{A}, \mathcal{W}, \mathcal{R}, P_1, P_2, P_3, f_s, \mu_0 \rangle$, where $\mathcal{S}, \mathcal{M}, \mathcal{A}, \mathcal{W}, \mathcal{R}, P_2, P_3, \mu_0$ denote the same meanings as they have in the general CMDP for unobserved confounders in Section 2, $P_1(r|s, w, m, s')$ denotes the reward distribution, and $f_s(s, m, \delta_s)$ denotes the next state transition function, in which δ_s denotes the error term in f_s .

The corresponding SCM in the offline setting can be defined as a four-tuple $\langle U, V, F, P_e \rangle$, where U, V, P_e denote the same meanings as they have in Section 2, and F includes the reward distribution $P_1(r|s, w, m, s')$, the confounder transition distribution $P_2(w|s)$, the intermediate state transition distribution $P_3(m|s, a)$, the next state transition function $f_s(s, m, \delta_s)$, and the behavior policy $\pi_b(a|s, w)$. The positivity assumption here is the same as the positivity assumption in Section 2.

The corresponding SCM in the online setting can be defined as another four-tuple $\langle U, V, F, P_e \rangle$, where F includes the reward distribution $P_1(r|s, w, m, s')$, the confounder transition distribution $P_2(w|s)$, the intermediate state transition distribution $P_3(m|s, a)$, the next state transition function $f_s(s, m, \delta_s)$, and the policy $\pi(a|s)$.

Based on the CMDP and the corresponding SCMs, we can derive Proposition 5 and Proposition 6.

Proposition 5. *Under the definitions of the CMDP and SCMs in this subsection, it holds that*

$$\begin{aligned}
 L_2(\phi, \mathcal{D}_{\text{off}}) &\triangleq \mathbb{E}_{s, a \sim \mathcal{D}_{\text{off}}} [\mathbb{E}_{s', r \sim \bar{P}(\cdot, \cdot | s, a)} [f_\phi(s, a, s', r) + h_\phi(s, a)]] \\
 &= \mathbb{E}_{s, a \sim \mathcal{D}_{\text{off}}, \delta_s \sim P_e} \left[\mathbb{E}_{r, m \sim \hat{P}(\cdot, \cdot | s, a)} [\bar{d}_1(\tau) f_\phi(s, a, f_s(s, m, \delta_s), r) + h_\phi(s, a)] \right] \\
 &= \mathbb{E}_{s, a, s', r, m \sim \mathcal{D}_{\text{off}}} [\bar{d}_1(\tau) f_\phi(s, a, s', r) + h_\phi(s, a)],
 \end{aligned} \tag{19}$$

where $\bar{d}_1(\tau)$ is defined as follows:

$$\bar{d}_1(\tau) = \frac{\sum_{a'} \hat{P}(r|m, a', s) \hat{P}(a'|s)}{\hat{P}(r|m, a, s)}. \tag{20}$$

Proof. The proof of this proposition is similar to the proof of Proposition 1 in Appendix A, and thus is omitted. \square

Proposition 6. *Under the definitions of the CMDP and SCMs in this subsection, the loss function of the resampling method (i.e., Equation 21) is asymptotically equal to that of the reweighting method as in Equation 22 provided that the dataset is large enough.*

$$L_3(\phi, \mathcal{D}_{\text{off}}) \triangleq \mathbb{E}_{I \sim \bar{p}_1} [f_\phi(s_I, a_I, s'_I, r_I) + h_\phi(s_I, a_I)], \quad (21)$$

where $\bar{p}_1(I = i) = \bar{d}_{1,i} / \sum_{j=1}^N \bar{d}_{1,j}$, and $\bar{d}_{1,i}$ is a shorthand for $\bar{d}_1(s_i, m_i, a_i, s'_i, r_i)$.

$$\lim_{N \rightarrow \infty} (L_3(\phi, \mathcal{D}_{\text{off}}) - L_2(\phi, \mathcal{D}_{\text{off}})) = 0 \quad (22)$$

Proof. The proof of this proposition is similar to the proof of Proposition 2 in Appendix A, and thus is omitted. \square

D.2 The Confounder Exists Only between the Action and Next State

The CMDP for the second specific case of unobserved confounders can be denoted by a nine-tuple $\langle \mathcal{S}, \mathcal{M}, \mathcal{A}, \mathcal{W}, \mathcal{R}, P_1, P_2, P_3, f_r, \mu_0 \rangle$, where $\mathcal{S}, \mathcal{M}, \mathcal{A}, \mathcal{W}, \mathcal{R}, P_2, P_3, \mu_0$ denote the same meanings as they have in the general CMDP for unobserved confounders in Section 2, $P_1(s'|s, w, m)$ denotes the next state transition distribution, and $f_r(s, m, \delta_r)$ denotes the reward function, in which δ_r denotes the error term in f_r .

The corresponding SCM in the offline setting can be defined as a four-tuple $\langle U, V, F, P_e \rangle$, where U, V, P_e denote the same meanings as they have in Section 2, and F includes the next state transition distribution $P_1(s'|s, w, m)$, the confounder transition distribution $P_2(w|s)$, the intermediate state transition distribution $P_3(m|s, a)$, the reward function $f_r(s, m, \delta_r)$, and the behavior policy $\pi_b(a|s, w)$. The positivity assumption here is the same as the positivity assumption in Section 2.

The corresponding SCM in the online setting can be defined as another four-tuple $\langle U, V, F, P_e \rangle$, where F includes the next state transition distribution $P_1(s'|s, w, m)$, the confounder transition distribution $P_2(w|s)$, the intermediate state transition distribution $P_3(m|s, a)$, the reward function $f_r(s, m, \delta_r)$, and the policy $\pi(a|s)$.

Based on the CMDP and the corresponding SCMs, we can derive Proposition 7 and Proposition 8.

Proposition 7. *Under the definitions of the CMDP and SCMs in this subsection, it holds that*

$$\begin{aligned} L_2(\phi, \mathcal{D}_{\text{off}}) &\triangleq \mathbb{E}_{s, a \sim \mathcal{D}_{\text{off}}} [\mathbb{E}_{s', r \sim \bar{P}(\cdot, \cdot | s, a)} [f_\phi(s, a, s', r) + h_\phi(s, a)]] \\ &= \mathbb{E}_{s, a \sim \mathcal{D}_{\text{off}}, \delta_r \sim P_e} \left[\mathbb{E}_{s', m \sim \hat{P}(\cdot, \cdot | s, a)} \left[\tilde{d}_1(\tau) f_\phi(s, a, s', f_r(s, m, \delta_r)) + h_\phi(s, a) \right] \right] \\ &= \mathbb{E}_{s, a, s', r, m \sim \mathcal{D}_{\text{off}}} \left[\tilde{d}_1(\tau) f_\phi(s, a, s', r) + h_\phi(s, a) \right], \end{aligned} \quad (23)$$

where $\tilde{d}_1(\tau)$ is defined as follows:

$$\tilde{d}_1(\tau) = \frac{\sum \hat{P}(s' | m, a', s) \hat{P}(a' | s)}{\hat{P}(s' | m, a, s)}. \quad (24)$$

Proof. The proof of this proposition is similar to the proof of Proposition 1 in Appendix A, and thus is omitted. \square

Proposition 8. *Under the definitions of the CMDP and SCMs in this subsection, the loss function of the resampling method (i.e., Equation 25) is asymptotically equal to that of the reweighting method as in Equation 26 provided that the dataset is large enough.*

$$L_3(\phi, \mathcal{D}_{\text{off}}) \triangleq \mathbb{E}_{I \sim \bar{p}_1} [f_\phi(s_I, a_I, s'_I, r_I) + h_\phi(s_I, a_I)], \quad (25)$$

where $\bar{p}_1(I = i) = \tilde{d}_{1,i} / \sum_{j=1}^N \tilde{d}_{1,j}$, and $\tilde{d}_{1,i}$ is a shorthand for $\tilde{d}_1(s_i, m_i, a_i, s'_i, r_i)$.

$$\lim_{N \rightarrow \infty} (L_3(\phi, \mathcal{D}_{\text{off}}) - L_2(\phi, \mathcal{D}_{\text{off}})) = 0 \quad (26)$$

Proof. The proof of this proposition is similar to the proof of Proposition 2 in Appendix A, and thus is omitted. \square

E Complete Empirical Results

The task settings of EmotionalPendulum, WindyPendulum, EmotionalPendulum* and WindyPendulum* are shown in the following two subsections. The additional empirical results of WindyPendulum, where the confounders are unobserved in the offline data, verify the effectiveness of the deconfounding methods proposed in Section 3. In contrast, the additional empirical results of WindyPendulum*, where the confounders are partially observed in the offline data, verify the effectiveness of the deconfounding methods proposed in Appendix B. In each subsection, we first describe the causal models of the offline data in the four benchmark tasks, and then compare BC, the original offline RL algorithms and the offline RL algorithms combined with our deconfounding methods in different task settings. The task settings follow Pendulum in OpenAI Gym except for the settings described in each subsection.

E.1 Unobserved Confounders

The causal model in the offline setting, which corresponds to EmotionalPendulum for unobserved confounders, is described as follows. In this causal model, $w_1 \in \{\text{True}, \text{False}\}$ represents whether the human sitting in the free end of the pendulum has negative emotions, $w_2 \in \{\text{True}, \text{False}\}$ represents whether the human has negative expressions, $s = (x, y, v)$ represents the Cartesian coordinates (x, y) and angular velocity (v) of the free end of the pendulum, the action $a \in \{-2, -1, 0, 1, 2\}$ represents the torque that the human wants to apply to the free end of the pendulum, the intermediate state $m \in \{-2, -1, 0, 1, 2\}$ represents the actual torque applied to the free end, and $r = r_o + r_a$ represents the reward where r_o represents the original reward in Pendulum of OpenAI Gym, and r_a represents the additional reward which is used to encourage the human with negative expressions. Note that the coordinates (x, y) are measured by a sensor which vibrates slightly at a distance of 1m from the fixed end of the pendulum, i.e., $x = \cos(\theta) \times l, y = \sin(\theta) \times l$ where θ denotes the angle in radians and $l \in (0.5, 1.5)$ denotes the truncated normal distribution with the mean $\mu = 1$ and the variance $\sigma = 0.01$.

The offline data generation process of this causal model is described as follows. The odds that the human does not have negative emotions are $odds_1 = \Pr(w_1 = \text{False}) / \Pr(w_1 = \text{True})$. If the human has negative emotions, he/she is most likely to have negative expressions, i.e., $\Pr(w_2 = \text{True}|w_1 = \text{True}) = 0.99, \Pr(w_2 = \text{False}|w_1 = \text{True}) = 0.01, \Pr(w_2 = \text{True}|w_1 = \text{False}) = 0.01, \Pr(w_2 = \text{False}|w_1 = \text{False}) = 0.99$. An agent is trained using the SAC algorithm in an environment where w_1, w_2 and s are observable for 300000 learning steps. This agent will be used to simulate the human in a rational state, and give the rational action \bar{a} at each step. We assume that the human may feel afraid and decide to slow down (i.e., $a = \tilde{a}$) if the speed is too fast (i.e., if the speed is above the threshold $|v| > v_T$), and the human may feel boring and decide to speed up (i.e., $a = \hat{a}$) if the speed is too slow (i.e., if $|v| \leq v_T$). Specifically, $\Pr(a = \bar{a}|w_1 = \text{False}) = 1, \Pr(a = \bar{a}|w_1 = \text{True}, v = 0) = 1, \Pr(a = \hat{a}|w_1 = \text{True}, |v| \leq v_T, v \neq 0) = I_{p,1}, \Pr(a = \bar{a}|w_1 = \text{True}, |v| \leq v_T, v \neq 0) = 1 - I_{p,1}, \Pr(a = \tilde{a}|w_1 = \text{True}, |v| > v_T) = I_{p,1}, \Pr(a = \bar{a}|w_1 = \text{True}, |v| > v_T) = 1 - I_{p,1}$, where $I_{p,1}$ denotes the probability of the human choosing irrational actions when he/she has negative emotions. The action $a \in \{-2, -1, 0, 1, 2\}$ influences the next state $s' \in \mathcal{S}$ through the intermediate state $m \in \{-2, -1, 0, 1, 2\}$. In most cases, m is equal to a (i.e., $\Pr(m = a) = 1 - p_{fail} + p_{fail}/5.$). However, in some cases, the human/agent fails to control the pendulum and m randomly chooses an action (i.e., $\forall \tilde{m} \neq a, \Pr(m = \tilde{m}) = p_{fail}/5.$). The environment will return an extra reward to encourage the human if his/her expressions are negative (i.e., r_a is subject to $N(10, 1)$ if $w_2 = \text{True}$, and is subject to $N(0, 1)$ if $w_2 = \text{False}$). The transition function in EmotionalPendulum is $\theta', v' = g(m)$, where θ' denotes the angle of the next state, v' denotes the angular velocity of the next state, and g denotes the original transition function in Pendulum of OpenAI Gym. The human interacts with the environment for 100000 steps to generate offline data.

The causal model in the offline setting, which corresponds to WindyPendulum for unobserved confounders, is described as follows. In this causal model, $w_2 \in \{0, 1, 2\}$ represents the direction of the wind, where 0 represents the wind from right to left, 1 represents no wind and 2 represents the wind from left to right, $w_1 \in \{\text{True}, \text{False}\}$ represents whether the human is afraid because of the wind, s, a and m represent the same meanings as s, a and m in EmotionalPendulum, and $r = r_o + r_a$ represents the reward, where r_o represents the original reward in Pendulum of OpenAI Gym, and r_a represents the additional reward used to encourage the human if a strong wind exists.

The offline data generation process of this causal model is described in the following. The odds of no wind are $odds_2 = \Pr(w_2 = 1) / (\Pr(w_2 = 0) + \Pr(w_2 = 2))$. If there is a gust of wind, the human will get scared, i.e., $\Pr(w_1 = \text{True}|w_2 \neq 1) = 1$. We use the SAC algorithm to train an agent in an environment where w_2 and s are observable for 300000 learning steps. This agent will be used to simulate the human in the rational state, and give the rational action \bar{a} at each step. We assume that the human in a state of fear may decide to slow down (i.e., $a = \tilde{a}$), and may choose a force opposite to the component of the wind force along the tangent (i.e., $a = \hat{a}$). Specifically, $\Pr(a = \bar{a}|w_1 = \text{False}) = 1, \Pr(a = \bar{a}|w_1 = \text{True}) = 1 - I_{p,2}, \Pr(a = \hat{a}|w_1 = \text{True}) = I_{p,2}/2, \Pr(a = \tilde{a}|w_1 = \text{True}) = I_{p,2}/2$, where $I_{p,2}$ denotes the probability that the human in a state of fear chooses irrational actions. The causal mechanism that generates m is the same as that in EmotionalPendulum. The environment will return an extra reward to encourage the human if there is a strong wind, i.e., r_a is subject to $N(10, 1)$ if $w_2 \neq 1$, and is subject to $N(0, 1)$ if $w_2 = 1$. The transition function in WindyPendulum is $\theta', v' = g(m - f_w \times \cos(\theta))$, where θ', v' and g denote the same meanings as θ', v' and g in EmotionalPendulum and f_w denotes the wind force as shown in Equation 27. Offline data are generated from 100000 steps of the human interacting with the environment.

$$f_w = \begin{cases} -5 & w_2 = 0 \\ 0 & w_2 = 1 \\ 5 & w_2 = 2 \end{cases} \quad (27)$$

As shown in Figure 10 and Figure 11, the offline RL algorithms combined with our deconfounding methods learn faster than the original offline RL algorithms under different settings of WindyPendulum for unobserved confounders, which verifies the robustness of our deconfounding methods. Since the human may adopt irrational actions in our tasks, his/her behavior policy is not good, and thus BC performs poorly in our tasks. The empirical results in Figure 10 and Figure 11 show that BC performs worse than the offline RL algorithms combined with our deconfounding methods.

Ablation study Figure 12 and Figure 13 provide an ablation study of the center sampling method k -means [MacQueen, 1967; Lloyd, 1982]. In the process of estimating the conditional probability densities using LSCDE, we need to select center points

for the kernel functions. DQN_RW and DQN_RS denote the deconfounding RL algorithms that use k -means clustering to determine k kernel centers. DQN_RW* and DQN_RS* denote the deconfounding RL algorithms that randomly select k points as kernel centers. Other algorithms are denoted similarly. Clearly, the deconfounding RL algorithms using the center sampling method k -means perform better than or similarly to the deconfounding RL algorithms that randomly select k points as kernel centers.

E.2 Partially Observed Confounders

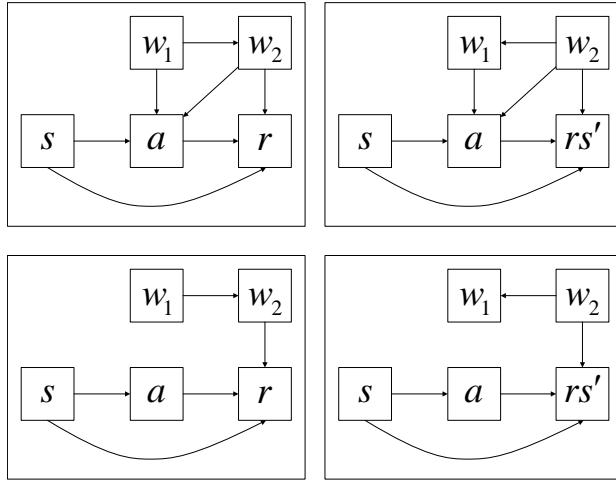


Figure 9: **Left:** the causal graphs depicting the offline and online data generating processes in EmotionalPendulum*. **Right:** the causal graphs depicting the offline and online data generating processes in WindyPendulum*. In both tasks, the confounders in the offline data are partially observable.

The causal graphs of EmotionalPendulum* and WindyPendulum* for partially observed confounders are shown in Figure 9. It is obvious that these causal graphs are special cases of the causal graphs described in Appendix B.1. The only difference between the causal models of the tasks for unobserved confounders and partially observed confounders is that there is no intermediate state m intercepting every directed path from a to s' anymore. In other words, the controller of the pendulum never fails, i.e., the action that the human wants to take is equal to the actual action executed by the machine. Meanwhile, the transition functions are changed correspondingly. In EmotionalPendulum*, $\theta', v' = g(a)$. In WindyPendulum*, $\theta', v' = g(a - f_w \times \cos(\theta))$.

Similar to EmotionalPendulum and WindyPendulum, in EmotionalPendulum* and WindyPendulum*, some sensors are used to collect the confounded offline data generated in the human-environment interaction process. The environmental information o_2 in these offline data includes s and a subset u of the confounder. In EmotionalPendulum*, $u = \{w_2\}$ where w_2 represents whether the human has negative expressions. In WindyPendulum*, $u = \{w_2\}$ where w_2 represents the direction of the wind. Except for what we have described above, the tasks for unobserved confounders and partially observed confounders are the same.

The empirical results in Figure 14 and Figure 15 demonstrate that the offline RL algorithms combined with our deconfounding methods learn faster than the original offline RL algorithms under different settings of WindyPendulum* for partially observed confounders, and thus verify the robustness of our deconfounding methods. As shown in Figure 14 and Figure 15, BC performs worse than the offline RL algorithms combined with our deconfounding methods.

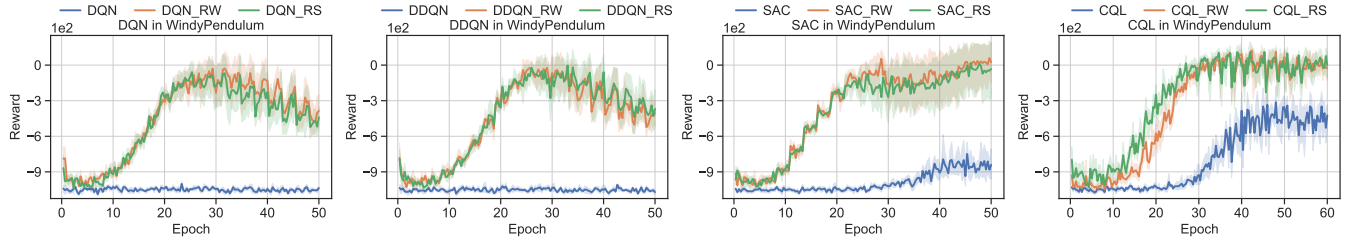


Figure 10: Performance of the deep RL algorithms with and without our deconfounding methods in WindyPendulum. The optimal average reward of BC over 50 epochs is -987.4. The rewards are tested over 20 episodes every 1000 learning steps. We divide the 50 epochs into 10 parts, and calculate the average reward of BC in each part. Finally, we take the largest average reward in all parts as the optimal average reward of BC. The task settings of this figure are as follows: $p_{fail} = 0.1$, $I_{p,2} = 0.9$, $odds_2 = 2$.

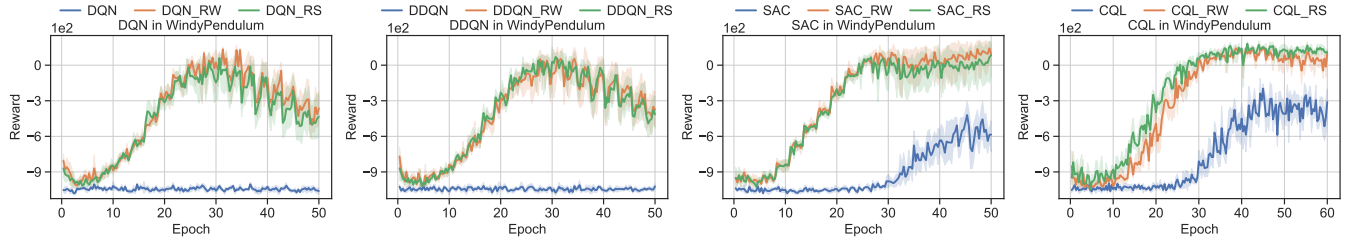


Figure 11: Performance of the deep RL algorithms with and without our deconfounding methods in WindyPendulum. The optimal average reward of BC over 50 epochs is -916.1. The task settings of this figure are as follows: $p_{fail} = 0.1$, $I_{p,2} = 0.85$, $odds_2 = 2$.

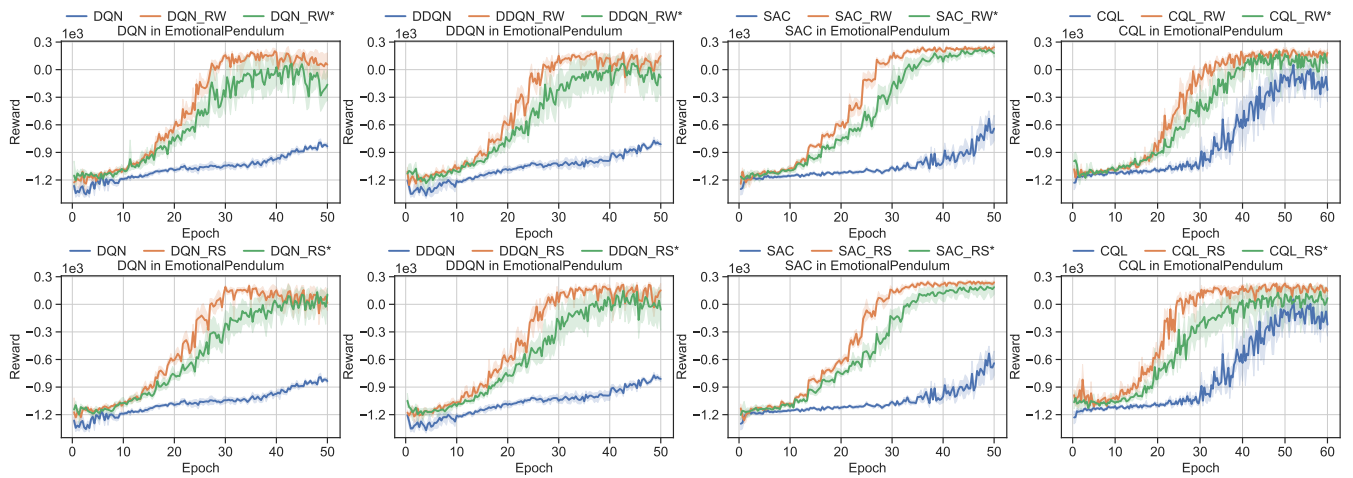


Figure 12: Performance of the deconfounding RL algorithms that use k -means clustering to determine k kernel centers and the deconfounding RL algorithms that randomly select k points as kernel centers in EmotionalPendulum. The task settings of this figure are described in Appendix C.

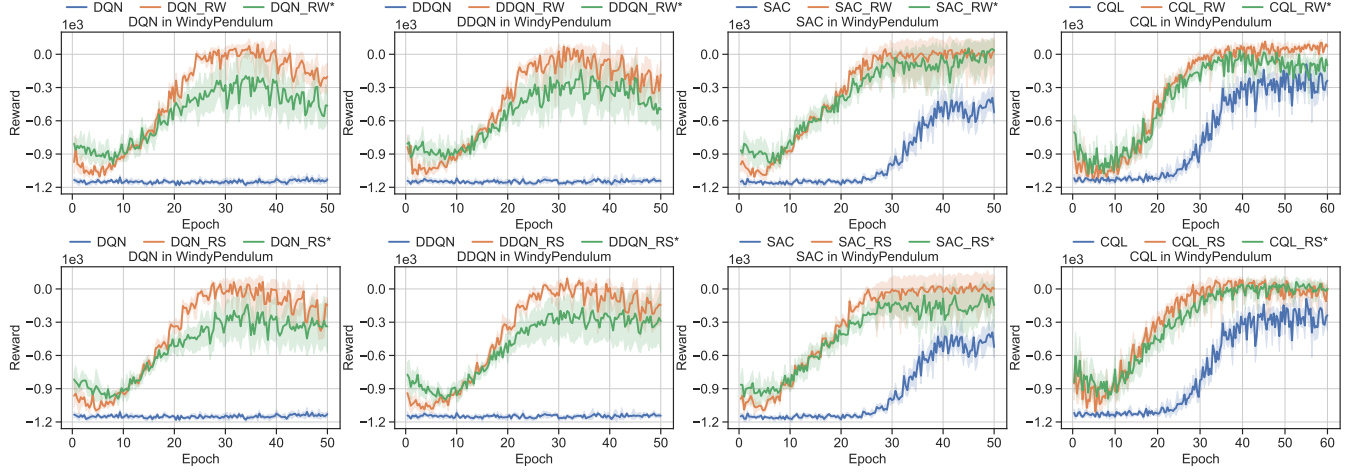


Figure 13: Performance of the deconfounding RL algorithms that use k -means clustering to determine k kernel centers and the deconfounding RL algorithms that randomly select k points as kernel centers in WindyPendulum. The task settings of this figure are described in Appendix C.

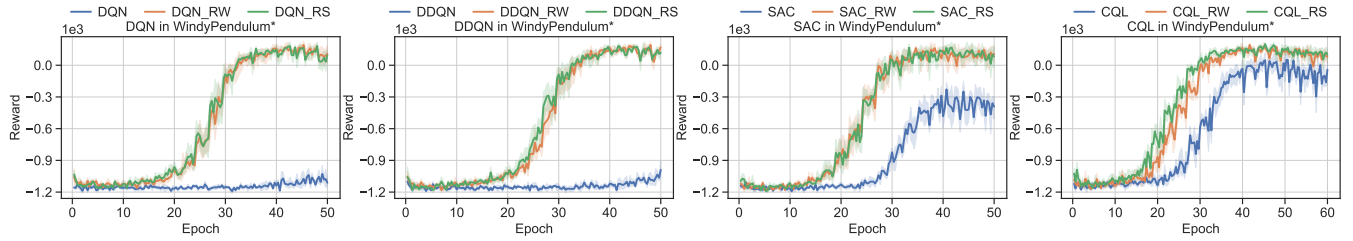


Figure 14: Performance of the deep RL algorithms with and without our deconfounding methods in WindyPendulum*. The optimal average reward of BC over 50 epochs is -826.5. The task settings of this figure are as follows: $I_{p,2} = 0.85$, $odds_2 = 2.5$.

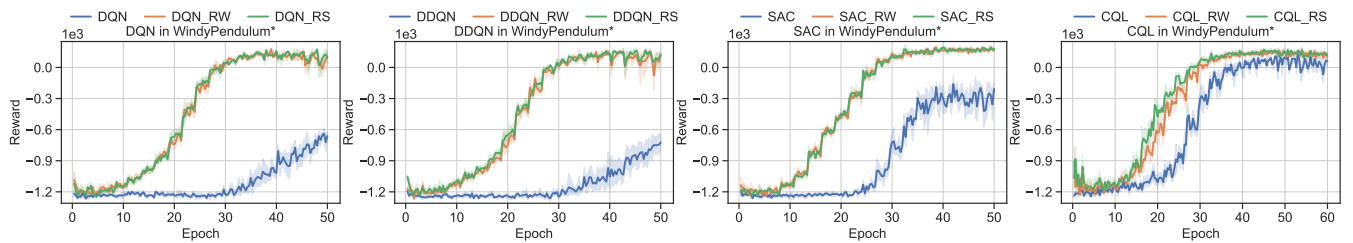


Figure 15: Performance of the deep RL algorithms with and without our deconfounding methods in WindyPendulum*. The optimal average reward of BC over 50 epochs is -432.9. The task settings of this figure are as follows: $I_{p,2} = 0.85$, $odds_2 = 3$.